

STAR FORMATION AND EXTINCTION IN REDSHIFT $Z \sim 2$ GALAXIES: INFERENCES FROM *SPITZER* MIPS OBSERVATIONS¹

NAVEEN A. REDDY², CHARLES C. STEIDEL², DARIO FADDA³, LIN YAN³, MAX PETTINI⁴, ALICE E. SHAPLEY⁵, DAWN K. ERB⁶, AND KURT L. ADELBERGER⁷

Received 2005 October 06; Accepted 2006 February 23

ABSTRACT

Using very deep *Spitzer* MIPS 24 μm observations, we present an analysis of the bolometric luminosities and UV extinction properties of more than 200 spectroscopically identified, optically selected (U_nGR) $z \sim 2$ galaxies in the GOODS-N field. The large spectroscopic sample of rest-UV selected galaxies is supplemented with photometrically identified near-IR-selected (“BzK” and “DRG”) galaxies and sub-mm sources at similar redshifts in the same field, providing a representative collection of relatively massive ($M^* > 10^{10} M_\odot$) galaxies at high redshifts. We focus on the redshift range $1.5 < z < 2.6$, for which the 24 μm observations provide a direct measurement of the strength of the mid-IR PAH features in the galaxy spectra; the rest-frame 5 – 8.5 μm luminosities ($L_{5-8.5\mu\text{m}}$) are particularly tightly constrained for the objects in our sample with precise spectroscopic redshifts. We demonstrate, using stacked X-ray observations and a subset of galaxies with $H\alpha$ measurements, that $L_{5-8.5\mu\text{m}}$ provides a reliable estimate of L_{IR} for most star forming galaxies at $z \sim 2$. We show that the range of L_{IR} in the optical/near IR-selected samples considered extends from $\simeq 10^{10} L_\odot$ to $> 10^{12} L_\odot$, with a mean $\langle L_{\text{IR}} \rangle \simeq 2 \times 10^{11} L_\odot$. The LIRG population at $z \sim 2$ is essentially the same population of galaxies that are selected by their optical/near-IR colors. Objects with LIRG to ULIRG luminosities are present over the full range of stellar masses in the samples, from $2 \times 10^9 M_\odot$ to $5 \times 10^{11} M_\odot$. We use the MIPS 24 μm observations for an independent examination of dust extinction in high redshift galaxies, and demonstrate that, as in the local universe, the obscuration ($\frac{L_{\text{IR}}}{L_{1600}}$) is strongly dependent on bolometric luminosity, and ranges in value from < 1 to ~ 1000 within the sample considered. However, the obscuration is ~ 10 times smaller at a given L_{bol} (or, equivalently, a similar level of obscuration occurs at luminosities ~ 10 times larger) at $z \sim 2$ than at $z \sim 0$. We show that the values of L_{IR} and obscuration inferred from the UV spectral slope β generally agree well with the values inferred from $L_{5-8.5\mu\text{m}}$ for $L_{\text{bol}} < 10^{12} L_\odot$. As found previously by several investigators, for “ultraluminous” objects with $L_{\text{bol}} > 10^{12} L_\odot$ it is common for UV-based estimates to underpredict L_{IR} by a factor of $\sim 10 - 100$. Using the specific star formation rate of galaxies (SFR per unit stellar mass) as a proxy for cold gas fraction, we find a wide range in the evolutionary state of galaxies at $z \sim 2$, from galaxies that have just begun to form stars to those which have already accumulated most of their stellar mass and are about to become, or already are, passively-evolving.

Subject headings: cosmology: observations — dust, extinction — galaxies: evolution — galaxies: high redshift — galaxies: stellar content — infrared: galaxies

1. INTRODUCTION

The most direct method currently available for tracing the bolometric luminosities of high redshift star-forming galaxies ($z \gtrsim 2$) has been from their submil-

limeter emission (e.g., Smail et al. 1997; Hughes et al. 1998; Barger et al. 1998). Unfortunately, current sensitivity limits of bolometers and submillimeter wave interferometers allow for only the most luminous starburst galaxies to be detected at high redshifts via their dust emission. Further compounding the problem is the coarse spatial resolution provided by such instruments, making it difficult to distinguish the counterpart(s) to the submillimeter emission for subsequent followup, although the recently developed method of radio-detection has been a breakthrough in alleviating this problem for most, but not all, bright submillimeter galaxies (e.g., Chapman et al. 2005). Regardless, the dust properties of the vast majority of star-forming galaxies at high redshift remained uninvestigated until recently.

The rest-frame far-infrared (FIR) wavelength region is still inaccessible for the *typical* galaxy at redshifts $z \gtrsim 1$, so we must look to other portions of the spectrum to directly examine dust properties. Our understanding of the mid-IR properties of local and high redshift galaxies advanced considerably with the launch of the

¹ Based, in part, on data obtained at the W.M. Keck Observatory, which is operated as a scientific partnership among the California Institute of Technology, the University of California, and NASA, and was made possible by the generous financial support of the W.M. Keck Foundation. Also based in part on observations made with the *Spitzer* Space Telescope, which is operated by the Jet Propulsion Laboratory, California Institute of Technology under a contract with NASA.

² California Institute of Technology, MS 105–24, Pasadena, CA 91125

³ *Spitzer* Science Center, California Institute of Technology, MS 220–6, Pasadena, CA 91126

⁴ Institute of Astronomy, Madingley Road, Cambridge CB3 0HA, UK

⁵ Department of Astrophysical Sciences, Peyton Hall-Ivy Lane, Princeton, NJ 08544

⁶ Harvard-Smithsonian Center for Astrophysics, 60 Garden Street, Cambridge, MA 02138

⁷ McKinsey & Company, 1420 Fifth Avenue, Suite 3100, Seattle, WA 98101

Infrared Space Observatory (ISO), which was sensitive enough to detect the mid-IR emission of $10^{11} L_{\odot}$ galaxies at $z \sim 1$ (e.g., Flores et al. 1999; Elbaz et al. 2002; Pozzi et al. 2004; Rowan-Robinson et al. 2004). These observations revealed the almost ubiquitous presence of mid-IR dust emission features in star forming galaxies in both the local and $z \sim 1$ universe, and suggested the possibility of using the mid-IR dust emission of galaxies as a tracer of bolometric luminosity (Boselli et al. 1998; Adelberger & Steidel 2000; Dale et al. 2000; Helou et al. 2000; Förster Schreiber et al. 2003).

These advances now continue with the highly successful *Spitzer* Space Telescope, providing the same sensitivity as ISO in probing dust emission from $10^{11} L_{\odot}$ galaxies at $z \sim 2$. The progress made with *Spitzer* is particularly important for studying galaxies at $z \sim 2$ because this epoch was until recently largely uninvestigated, yet is believed to be the most active in terms of star formation and the build up of stellar and black hole mass (e.g., Dickinson et al. 2003; Rudnick et al. 2003; Madau et al. 1996; Lilly et al. 1996; Steidel et al. 1999; Shaver et al. 1996; Fan et al. 2001; Di Matteo et al. 2003; Giavalisco et al. 1996). The sensitivity afforded by the *Spitzer* MIPS instrument allows us to examine the *typical* L^* galaxy at $z \sim 2$, rather than a limited slice of the most luminous population, a problem which, as alluded to before, limits the usefulness of submillimeter observations.

It is fortuitous that the rest-frame mid-IR spectral features observed in local and $z \sim 1$ star-forming galaxies are redshifted into the *Spitzer* IRS spectral and MIPS imaging passbands at $z \sim 2$. The mid-IR spectral region from 3 – 15 μm is rich with emission lines believed to arise from the stochastic heating of small dust grains by UV photons (see review by Genzel & Cesarsky 2000). These unidentified infrared bands (UIBs) are generally attributed to the C = C and C – H stretching and bending vibrational modes of a class of carbonaceous molecules called polycyclic aromatic hydrocarbons (PAHs; e.g., Puget & Leger 1989; Tielens et al. 1999), which we assume hereafter. In the typical spectrum of a star-forming galaxy, these PAH emission lines, along with various fine-structure metal and HI recombination lines (e.g., Sturm et al. 2000), are superposed on a mid-IR continuum thought to result from dust emission from very small grains, or VSGs (Desert et al. 1990). In star-forming galaxies, the global PAH emission is mainly attributed to UV radiation from OB stars and has been found to correlate with global star formation rate (e.g., Förster Schreiber et al. 2004b; Förster Schreiber et al. 2003; Roussel et al. 2001), although variations with ionizing intensity and metallicity are also observed (e.g., Engelbracht et al. 2005; Hogg et al. 2005; Alonso-Herrero et al. 2004; Helou et al. 2001; Normand et al. 1995).

Until now, the only way to estimate the bolometric luminosities of most galaxies at $z \sim 2$ independent of extinction was via their stacked X-ray and radio emission: unfortunately these data are not sufficiently sensitive to detect individual L^* galaxies at $z \sim 2$ (e.g., Reddy & Steidel 2004; Nandra et al. 2002; Brandt et al. 2001). The *Spitzer* data considered in this paper are useful in assessing the bolometric luminosities of galaxies on an individual basis. One is still limited because detailed

mid-IR spectroscopy is feasible only for the most luminous galaxies at $z \sim 2$ (e.g., Yan et al. 2005; Houck et al. 2005), but L^* galaxies at $z \sim 2$ (with $L_{\text{bol}} \sim 10^{11} L_{\odot}$) can be detected in deep 24 μm images. We employ MIPS 24 μm data to study the rest-frame mid-IR properties of optical and near-IR selected galaxies at redshifts $1.5 \lesssim z \lesssim 2.6$. We describe the optical, near-IR, X-ray, and mid-IR data in § 2 and 3. Our large sample of spectroscopic redshifts for optically-selected galaxies allows us to very accurately constrain the rest-frame mid-IR fluxes of $z \sim 2$ galaxies. In § 4, we describe our method for estimating photometric redshifts for near-IR samples of galaxies where spectroscopy is less feasible. The procedure for estimating infrared luminosities from MIPS data is outlined in § 5.1. We discuss the infrared luminosity distributions of 24 μm detected and undetected sources in § 5.2 and 5.3. The dust attenuation properties of optical and near-IR selected $z \sim 2$ galaxies and the correlation of these properties with bolometric luminosity are discussed in § 6 and § 7. The stellar populations and composite rest-frame UV spectral properties of faint 24 μm galaxies are discussed in § 8. In § 9 we examine in more detail the mid-IR properties of massive galaxies at $z \sim 2$. We conclude in § 10 by discussing the viability of optical and near-IR color criteria in selecting LIRGs and ULIRGs at $z \sim 2$ and what the *Spitzer* MIPS observations can reveal about the mass assembly of galaxies at high redshift. A flat Λ CDM cosmology is assumed with $H_0 = 70 \text{ km s}^{-1} \text{ Mpc}^{-1}$ and $\Omega_{\Lambda} = 0.7$.

2. SAMPLE SELECTION AND ANCILLARY DATA

2.1. Optical and Near-IR Selection

The star-forming galaxies studied here were drawn from the sample of $z \sim 2$ galaxies in the GOODS-N field selected based on their observed U_nGR colors to $\mathcal{R} = 25.5$ (Adelberger et al. 2004; Steidel et al. 2004). The optical images used for the selection of candidates cover an area $11' \text{ by } 15'$. We refer to “BM” and “BX” galaxies as those which are selected to be at redshifts $1.5 \lesssim z \lesssim 2$ and $2.0 \lesssim z \lesssim 2.6$, respectively (Adelberger et al. 2004; Steidel et al. 2004). In addition to BX/BM galaxies, we also consider galaxies selected using the $z \sim 3$ LBG criteria (Steidel et al. 2003). The BX/BM and LBG candidates make up our U_nGR , or optically, selected sample. We obtained rest-frame UV spectra with the blue channel of the Low Resolution Imaging Spectrograph (LRIS-B) on Keck I for 386 U_nGR candidates. The numbers of candidates and spectroscopically confirmed galaxies in the U_nGR sample are summarized in Table 1. The *spectroscopic* redshift distribution of U_nGR galaxies in the GOODS-N field is shown in Figure 1. For efficiency, we preferentially targeted for spectroscopy those U_nGR candidates with \mathcal{R} -band magnitudes in the range $\mathcal{R} = 22.5 - 24.5$ (AB units) and gave lower priorities for fainter objects where redshift identification is more difficult from absorption lines and brighter objects where the contamination fraction (from low redshift interlopers) is larger. The star formation rate distribution of spectroscopically-confirmed U_nGR galaxies is similar to that of all U_nGR galaxies in the targeted redshift range to $K_s = 21$ (Vega; Reddy et al. 2005; see also Steidel et al. 2004 for a discussion of spectroscopic bias of galaxy properties with respect to the photometric sample of U_nGR galaxies).

TABLE 1
PROPERTIES OF THE SAMPLES

Sample	Limits	N_c^a	N_x^b	ρ^c (arcmin $^{-2}$)	N_s^d	$\langle z \rangle^e$	N_g^f	f_m^g
U_nGR (BX/BM/LBG)	$\mathcal{R} < 25.5$	1571	23	10.2 ± 0.3	313	2.25 ± 0.33	219	0.65
BzK/SF	$K_s < 21.0$	221	32	3.1 ± 0.2	53	2.09 ± 0.34	82	0.82
BzK/PE	$K_s < 21.0$	17	4	0.24 ± 0.06	0	1.70 ± 0.20	13	0.54
DRG ^h	$K_s < 21.0$	73	19	1.0 ± 0.1	5	2.48 ± 0.35	24	0.71

^aNumber of candidates.

^bNumber of directly-detected X-ray sources, including spectroscopically-confirmed galaxies.

^cSurface density of candidates. Errors are computed assuming Poisson statistics.

^dNumber of spectroscopically confirmed objects with $z > 1.5$. Note that we only obtained spectra for those BzK and DRG galaxies that satisfy the U_nGR criteria.

^eMean redshift of sample for $z > 1.5$. For the BzK/PE sample, this is the mean redshift of the *photometric* redshift distribution observed for BzK/PE galaxies (e.g., Daddi et al. 2004; Reddy et al. 2005). For the DRGs, this is the mean redshift of the *spectroscopic* redshift distribution observed for DRGs with $z > 1.5$ in four of the fields of the $z \sim 2$ optical survey (Reddy et al. 2005).

^fNumber of non-AGN galaxies (i.e., those with no direct X-ray detections) with spectroscopic redshifts $1.5 < z < 2.6$. For the BzK/SF sample, this number includes both spectroscopically-confirmed BzK/SF galaxies (all of which are in the U_nGR sample) and those with secure photometric redshifts. For the BzK/PE sample, this includes all candidates without direct X-ray detections. For the DRG sample, this number includes galaxies with photometric redshifts $1.5 < z < 2.6$.

^gFraction of MIPS $24 \mu\text{m}$ detections to $8 \mu\text{Jy}$ (3σ) among the N_g galaxies.

^hThe DRG sample includes both star-forming galaxies and those with little star formation. As discussed in Reddy et al. (2005), those with spectra (i.e., those DRGs which also satisfy the U_nGR criteria) are likely to be currently forming stars.

Our deep near-IR J and K -band imaging, in addition to publicly available deep optical imaging, allows us to select both star-forming galaxies and those with little current star formation in the GOODS-N field. Details of the optical and near-IR images are provided in Reddy et al. (2005). The near-IR selection of star-forming galaxies is done using the criteria of Daddi et al. (2004), resulting in a “ BzK/SF ” sample (e.g., Daddi et al. 2004; Reddy et al. 2005). The near-IR selected samples of galaxies with very little current star formation are constructed by considering the BzK and $J - K_s$ colors of candidates satisfying the BzK/PE and Distant Red Galaxy (DRG) criteria (e.g., Reddy et al. 2005; Daddi et al. 2004; Franx et al. 2003). Approximately 70% of DRGs to $K_s = 21$ (Vega) have signatures of intense star formation (Papovich et al. 2005; Reddy et al. 2005; van Dokkum et al. 2004)⁸. The J and K band images cover a large area by near-IR standards ($\sim 8.5' \times 8.5'$), but are still less than half the area of the optical U_nGR images. The number of near-IR selected candidates and their surface densities are presented in Table 1. For the remaining analysis, we use AB units for optical (U_nGR) magnitudes and Vega units for near-IR (K_s) magnitudes.

2.2. X-Ray Data

The very deep *Chandra* X-ray data in the GOODS-N field (Alexander et al. 2003) allow for an independent means of assessing the presence of AGN in the samples, which can be quite significant for near-IR selected samples (Reddy et al. 2005). In addition, we can stack the X-ray data for those galaxies lying below the X-ray detection threshold to determine their average emission properties (e.g. Laird et al. 2005; Lehmer et al. 2005;

⁸ In order to ensure our sample is complete, we only consider DRGs to $K_s = 21$.

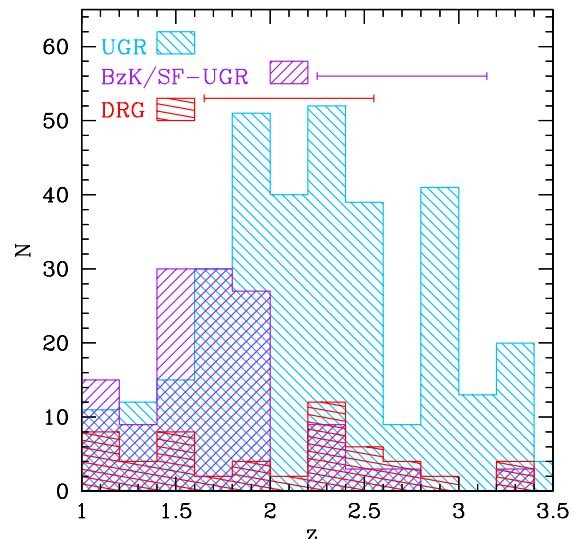


FIG. 1.— Spectroscopic redshift distribution of optically (i.e., U_nGR) selected galaxies, with typical error of $\sigma(z) = 0.002$. Also shown are arbitrarily normalized photometric redshift distributions of BzK/SF galaxies that do not satisfy the U_nGR criteria, and DRGs. The errorbars indicate the average uncertainty in photometric redshifts ($\sigma(z) = 0.45$) for the near-IR selected BzK galaxies and DRGs.

Reddy & Steidel 2004; Nandra et al. 2002; Brandt et al. 2001). The X-ray data and stacking methods are discussed in detail in Reddy & Steidel (2004) and Reddy et al. (2005). The numbers of directly-detected X-ray sources in each sample considered here are summarized in Table 1.

3. MID-IR DATA

The mid-IR data are obtained from the *Spitzer* Multi-band Imaging Photometer (MIPS) instrument. The 24

micron data were taken as part of the GOODS Legacy Survey (P.I.: M. Dickinson) between May 27 and June 6, 2004. They consist of 24 AORs (Astronomical Observation Requests) of approximately 3 hours each. The combined data reach a depth equivalent to ~ 10 hours integration at any point in the mosaicked image. The data are publicly available since August 2004 in the Spitzer archive. The basic calibrated data (BCD) produced by the Spitzer pipeline were used as the starting point for the data reduction. As explained in detail by Fadda (2006), there were several artifacts which added noise to the images, hampering the detection of faint sources. These artifacts include image latencies from previous observations of bright objects or image dark spots present on the pick-off mirror that are projected in different positions by the cryogenic scan mirror during observations. Other variations come from the variable zodiacal light. We have corrected each BCD image for these effects using the procedure described by Fadda (2006). The final mosaic consists of 7198 BCDs combined using MOPEX (Makovoz & Marleau 2005). The final reduced $24 \mu\text{m}$ mosaic of the GOODS-N region has a pixel size of $1''.275$ and covers the entirety of our optical U_nGR images and the measured 3σ depth is approximately $8 \mu\text{Jy}$. The large beam-size of MIPS ($\sim 5''.4$ at $24 \mu\text{m}$) combined with the effects of blending make aperture photometry impractical. Instead, we have chosen to use a PSF fitting method to extract $24 \mu\text{m}$ fluxes for our galaxies, similar to the method used to extract IRAC fluxes for galaxies as discussed in Shapley et al. (2005).

We first compute an empirical PSF using a two-pass approach. In the first pass, we take the median flux profile of several tens of distinct MIPS point sources across the mosaic to create a rough empirical PSF. This PSF is then used to subtract sources in proximity to the tens of MIPS point sources in order to better determine the PSF profile out to larger radii. This is important for the MIPS PSF which contains up to 20% of the point source flux in the Airy rings. The effects of source confusion are mitigated by employing the higher spatial resolution *Spitzer* IRAC data in the GOODS-N field to constrain the MIPS source positions. The empirical PSF, normalized to unit flux, is fit to these positions and the fluxes are extracted. The PSF used here extends to $15''.3$ radius, and we apply a 15% aperture correction based on the observed curves-of-growth of MIPS point source profiles from the First Look Survey.

The number of MIPS detections ($> 3 \sigma$) and non-detections in each sample are summarized in Table 1. Virtually all of the directly-detected X-ray sources are detected at $24 \mu\text{m}$ and all have optical/X-ray flux ratios indicating that AGN dominate the X-flux (Reddy et al. 2005). Submillimeter galaxies are often associated with direct X-ray detections (e.g., Alexander et al. 2005; Reddy et al. 2005) even though their bolometric luminosities may still be dominated by star-formation. Since we are primarily interested in the mid-IR emission as a tracer of star formation, we have excluded all directly-detected X-ray sources (almost all of which are AGN; Reddy et al. 2005) for most of the analysis, unless they happen to coincide with a radio-detected SMG from the Chapman et al. (2005) (SC05) sample. We caution that the resulting sample of 9 SMGs is not meant to be uniform or complete: $\sim 40\%$ of SMGs are not associ-

TABLE 2
LOCAL TEMPLATE GALAXIES

Name ^a	z^b	L_{IR} ($\times 10^{10} L_{\odot}$)
M82	0.000677	4.8
NGC253	0.000811	1.8
M83	0.001711	1.9
M51	0.002000	2.4
NGC1808	0.003319	3.8
NGC1097	0.004240	3.8
NGC1365	0.005457	8.7
NGC520	0.007609	6.5
NGC7714	0.009333	5.6
NGC3256	0.009386	40
NGC6240	0.024480	60
IRS9	1.83	1800

^aAll galaxies are compiled from Förster Schreiber et al. (2004a) and Roussel et al. (2001), except for IRS9 and NGC7714 which are taken from Yan et al. (2005). The bolometric luminosity of IRS9 is constrained within a factor of 2-3 (Yan et al. 2005).

^bRedshifts for local galaxies are obtained from NASA/IPAC Extragalactic Database (NED).

ated with radio sources, either because of their higher redshifts or radio faintness (e.g., Chapman et al. 2005; Smail et al. 2002). Furthermore, the submillimeter observations are not uniform over the field. Nonetheless, it is of obvious interest to at least compare the mid-IR properties of this limited set of radio-detected SMGs to those of galaxies in other samples.

The MIPS $24 \mu\text{m}$ filter directly samples the rest-frame luminosity from $5 - 8.5 \mu\text{m}$ ($L_{5-8.5\mu\text{m}}$) for redshifts $1.5 \lesssim z \lesssim 2.6$. We used the mid-IR spectral shapes of star-forming galaxies (listed in Table 2) as templates in order to K -correct the $24 \mu\text{m}$ fluxes to determine $L_{5-8.5\mu\text{m}}$. Figure 2 shows the expected $24 \mu\text{m}$ fluxes of the galaxies listed in Table 2 as a function of redshift. These galaxies were chosen to cover a large range in SFRs (from quiescent spiral galaxies to starbursts and LIRGs/ULIRGs). The mid-IR spectra are obtained from either ISO (for local galaxies; Förster Schreiber et al. 2004a) or *Spitzer* IRS (for $z \sim 2$ hyper-luminous galaxies; Yan et al. 2005) observations. Some properties of these galaxies are summarized in Table 2. The mid-IR spectrum of each galaxy is redshifted, convolved with the MIPS $24 \mu\text{m}$ filter, and the fluxes are normalized to have $L_{5-8.5\mu\text{m}} = 10^{10} L_{\odot}$ to produce the dotted curves in Figure 2. The small dispersion between the templates over redshifts $1.5 \lesssim z \lesssim 2.6$ reflects small changes in the broadband $24 \mu\text{m}$ fluxes of galaxies due to changes in the relative strengths of the various PAH emission lines and the ratio of PAH-to-continuum flux. The solid curve in the figure shows the average of all the template galaxies. The prominent peak at $z \approx 1.9$ is primarily due to the $7.7 \mu\text{m}$ feature shifting into the MIPS $24 \mu\text{m}$ filter.

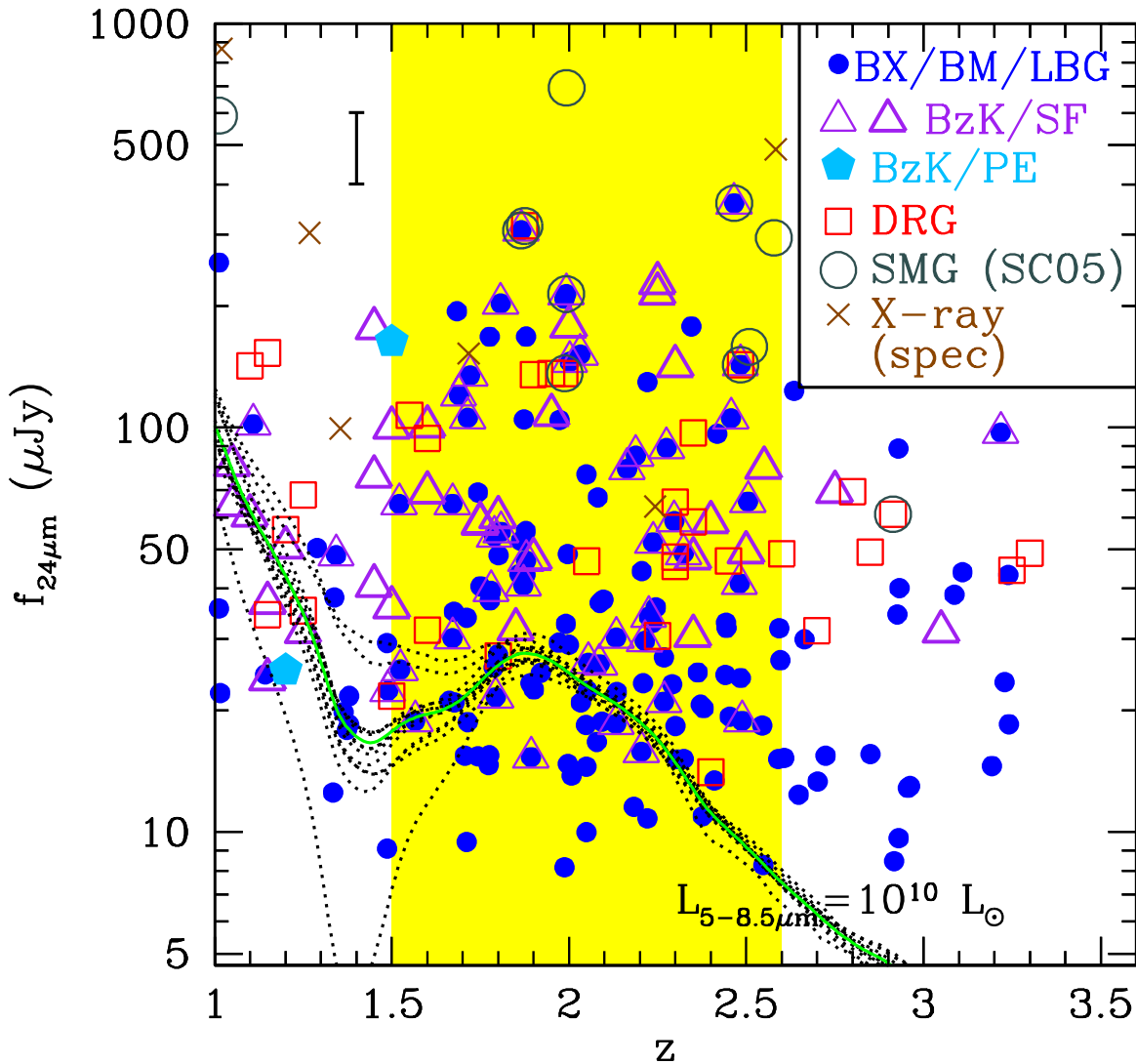


FIG. 2.— Expected 24 μm fluxes of the local and high redshift template galaxies summarized in Table 2 shown by the dotted curves, normalized so that $L_{5-8.5\mu\text{m}} = 10^{10} L_{\odot}$. The solid curve is the average over all the templates. Also shown are the observed fluxes of U_nGR (small points) and BzK/SF galaxies (thin triangles) with spectroscopic redshifts; and BzK/SF (thick triangles), BzK/PE (solid pentagons), and DRGs (open squares) with photometric redshifts. The typical error in photometric redshifts of DRG and BzK galaxies is $\sigma(z) \sim 0.45$. Radio-detected submillimeter galaxies to $S_{850\mu\text{m}} \sim 4.2$ mJy from Chapman et al. (2005) are shown by the open circles. We have removed directly-detected X-ray sources in the samples above, except for those in the SMG sample. Crosses denote hard-band X-ray sources with spectroscopic redshifts in the U_nGR sample. The vertical errorbar in the upper left-hand side of the figure shows the typical uncertainty in the 24 μm flux. The shaded region indicates the redshift range over which the MIPS 24 μm filter directly samples the rest-frame 7.7 μm PAH feature.

Figure 2 illustrates the sensitive dependence of the K -correction on the redshift (e.g., galaxies with a given observed $f_{24\mu\text{m}}$ can have a factor of 3 spread in $L_{5-8.5\mu\text{m}}$ depending on their redshift in the range $1.5 < z < 2.6$). Our large *spectroscopic* sample gives us the distinct advantage of knowing the *precise* redshifts for the optically selected galaxies, removing the added uncertainty introduced by photometric redshifts where the precise location of the PAH features with respect to the MIPS 24 μm filter is unknown, adding considerable uncertainty to the inferred infrared luminosities (e.g., Papovich et al. 2005). As we show below, the typical error in the photometric redshifts derived for near-IR selected galaxies (even when using data across a large baseline in wavelength, from UV through *Spitzer* IRAC), is $\sigma(z) \sim 0.5$. This error in redshift translates to at least a factor of three uncertainty in $L_{5-8.5\mu\text{m}}$.

Nonetheless, photometric redshifts are the only practical option for optically faint galaxies where spectroscopy is not feasible. This is true for many of the DRGs and BzK/PE galaxies. We supplement our spectroscopic database of optically selected galaxies with photometric redshifts of near-IR selected galaxies. We made use of the HyperZ code to determine photometric redshifts (Bolzonella et al. 2000). To quantify the uncertainties in photometric redshifts, we tested the code on U_nGR galaxies with spectroscopic redshifts, fitting to the $U_nBGVRIz + JK$ photometry. The $BVIz$ magnitudes are obtained from the v1.1 release of the GOODS ACS catalogs (Giavalisco et al. 2004). Errors in the optical U_nGR and near-IR JK magnitudes are determined from Monte Carlo simulations described by Erb et al. (2006b) and Shapley et al. (2005).

The χ^2 between the modeled and observed colors was

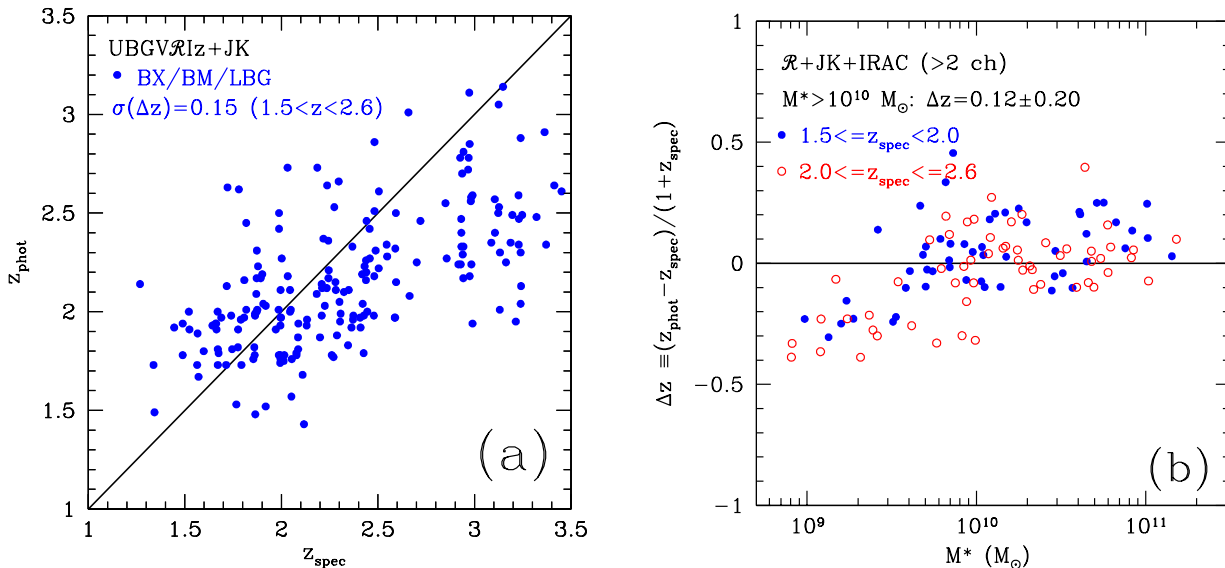


FIG. 3.— *Left panel:* Photometric versus spectroscopic redshifts for U_nGR galaxies. The solid line indicates $z_{\text{phot}} = z_{\text{spec}}$. *Right panel:* Δz , as defined in the text, as a function of stellar mass for galaxies with redshifts $1.5 \leq z < 2.0$ (solid circles) and $2.0 \leq z \leq 2.6$ (open circles). The figure only shows objects with $> 3 \sigma$ detections in at least two IRAC channels.

calculated for each galaxy for a number of different star formation histories (with exponential decay times $\tau = 10, 20, 50, 100, 200, 500, 1000, 2000,$ and 5000 Myr, and $\tau = \infty$) as a function of redshift. The best-fit photometric redshift is the redshift at which χ^2 is minimized. As a figure of merit of the resulting fit (and for easy comparison with other studies), we compute

$$\Delta z \equiv (z_{\text{phot}} - z_{\text{spec}}) / (1 + z_{\text{spec}}). \quad (1)$$

The results are shown in the left panel of Figure 3. The dispersion in Δz is $\sigma(\Delta z) \approx 0.15$ for galaxies with spectroscopic redshifts $1.5 < z < 2.6$. The actual error in redshift is typically $\sigma(z) \sim 0.45$. Both the Shapley et al. (2005) code (which uses Bruzual & Charlot (2003) models) and the Benítez (2000) code gave similar results. We found that adding *Spitzer* IRAC data does little to tighten the scatter between photometric and spectroscopic redshifts for most galaxies, reflecting the absence of any distinct features (e.g., strong spectral breaks) across the IRAC bands for $z \sim 2$ galaxies. We note from the left panel of Figure 3 that photometric redshifts systematically underestimate the true redshifts of $z > 3$ galaxies. This should not significantly affect our subsequent analysis since we only consider galaxies up to $z = 2.6$, and most of the *BzK*/SF and DRG galaxies have photometric redshifts $z_{\text{phot}} \lesssim 2.5$.

The IRAC data are nonetheless a powerful tool in discerning the more massive galaxies from the less massive ones. Since most of the optically-faint DRGs and *BzK*/PE galaxies are on average amongst the more massive galaxies at $z \sim 2$ (e.g., Figure 18 of Reddy et al. (2005)), we have incorporated the IRAC data in the photometric redshift fits. The right panel of Figure 3 shows Δz as a function of inferred stellar mass for U_nGR galaxies computed for the best-fit τ model, normalizing to the observed colors⁹. The scatter in Δz for galaxies with stellar masses $M^* \gtrsim 10^{10} M_{\odot}$ is $\sigma(\Delta z) \sim 0.20$, and we will assume this value for the error in photometric redshifts of

the DRG and *BzK*/PE galaxies. To extend the comparison presented by Reddy et al. (2005) between U_nGR and *BzK* selected samples of star-forming galaxies by examining their mid-IR properties, we compute photometric redshifts for *BzK*/SF galaxies that do not satisfy the U_nGR criteria. For the *BzK*/SF galaxies, we assume an error of $\sigma(\Delta z) \sim 0.15$, according to Figure 3a.

We obtained 51 secure photometric redshift fits for *BzK*/SF galaxies not selected by the U_nGR criteria (out of 95 such objects), and their (arbitrarily normalized) photometric redshift distribution is shown in Figure 1. Also shown is the (arbitrarily normalized) photometric redshift distribution for 28 (out of 49) non X-ray detected DRGs for which we were able to derive secure photometric redshifts $1 < z_{\text{phot}} < 3.5$. The remaining DRGs either have $z_{\text{phot}} < 1$ or $z_{\text{phot}} > 3.5$ (and are irrelevant to the analysis considered below) or had photometry that was inconsistent with the Bruzual & Charlot (2003) models considered here, resulting in a large χ^2 value between the model and observed colors. The DRGs examined here appear to span a very large range in redshift from $z \sim 1 - 3.5$, a result similar to that found by Papovich et al. (2005) for DRGs in the GOODS-South field. We obtained good photometric redshift fits for only two of the *BzK*/PE galaxies: one at $z \sim 1.2$ and the other at $z \sim 1.5$. We reiterate that for purposes of redshift identification, we only assumed the photometric redshifts for those galaxies for which we were able to obtain good SED fits (i.e., with $\chi^2 \approx 1$) to the observed data. There were a number of objects for which the photometric redshift errors were relatively large ($\delta z / (1 + z) \gtrsim 1$) or had derived redshifts that were much larger ($z > 4$) or smaller ($z < 1$) than of interest here, and we excluded such objects from our analysis. Hence, the photometric redshift distributions in Figure 1 should not be attributed to the populations as a whole. For the remaining analysis we consider only optically-selected galaxies with spectroscopic redshifts and near-IR selected galaxies with photometric redshifts between $1.5 \lesssim z \lesssim 2.6$ where the $24 \mu\text{m}$ fluxes directly trace the

⁹ We assume a Salpeter IMF in calculating the stellar mass.

flux at rest-frame $7.7 \mu\text{m}$. This is indicated by the shaded region in Figure 2.

5. INFRARED LUMINOSITIES OF OPTICAL, NEAR-IR, AND SUBMILLIMETER SELECTED GALAXIES AT $Z \sim 2$

5.1. Inferring Infrared Luminosities from $L_{5-8.5\mu\text{m}}$

The conversion between $L_{5-8.5\mu\text{m}}$ and infrared luminosity will largely depend on the assumed spectral template relating the mid-IR emission of galaxies to their total infrared luminosities. Fortunately, the deep X-ray data allow us to determine whether $L_{5-8.5\mu\text{m}}$ scales with infrared luminosity (or star formation rate) independent of any assumed template, adopting the local empirical relationship between X-ray and FIR luminosity for star-forming galaxies. Figure 4 shows the ratio of $L_{5-8.5\mu\text{m}}$ to stacked X-ray luminosity of (X-ray undetected) galaxies in bins of $L_{5-8.5\mu\text{m}}$: we only considered optically-selected galaxies with spectroscopic redshifts since it is for these galaxies which we are able to most accurately constrain the rest-frame X-ray luminosities. Since X-ray emission is sensitive to star formation on time-scales of $\gtrsim 100$ Myr (see § 6), Figure 4 shows results excluding galaxies with inferred ages < 100 Myr. Each bin contains 10 – 20 sources except the faintest bin which includes 45 galaxies undetected at $24 \mu\text{m}$ with ages > 100 Myr. The X-ray data for galaxies in each bin were stacked using the procedure described in Reddy et al. (2005). The mean value of the mid-IR-to-X-ray luminosity ratio is $\langle L_{5-8.5\mu\text{m}}/L_{2-10 \text{ keV}} \rangle \approx 251 \pm 41$. The X-ray luminosities of local star-forming galaxies are found to tightly correlate with their infrared emission for galaxies with $10^8 \lesssim L_{\text{FIR}} \lesssim 10^{12} L_{\odot}$ (e.g., Ranalli et al. 2003). Using the X-ray luminosity as a proxy for infrared luminosity therefore implies that the rest-frame mid-IR fluxes follow the total infrared luminosity (L_{IR}) for the vast majority of optically-selected galaxies at $z \sim 2^{10}$. The mid-IR fluxes must also follow the infrared luminosity for most near-IR selected star-forming galaxies as well given the large overlap (70% – 80%) between optical and near-IR selected samples of $z \sim 2$ star-forming galaxies (Reddy et al. 2005). As we show below, the conversion we assume between rest-frame mid-IR and infrared luminosities reproduces the average infrared luminosities predicted from stacked X-ray analyses (§ 6.1).

To quantify the relationship between rest-frame mid-IR and total infrared luminosity with a minimum number of assumptions, we have made use of the data compiled by Elbaz et al. (2002), which include IRAS 60 and $100 \mu\text{m}$ measurements and *ISO* observations of 149 local star-forming galaxies with L_{IR} in the range $10^9 \lesssim L_{\text{IR}} \lesssim 10^{12.6} L_{\odot}$. The mean and dispersion of the IR/MIR flux ratio for the sample of 149 galaxies is $\langle \log(L_{\text{IR}}/L_{5-8.5\mu\text{m}}) \rangle = 1.24 \pm 0.35$. Note the large 1σ dispersion of a factor of 2.2 in the IR/MIR flux ratio. The dispersion in the IR/MIR flux ratios between galaxies may be driven partly by changes in the mid-IR line strengths as the aromatic carriers are dehydrogenated and/or destroyed depending on the intensity of the ambient UV ionizing field (e.g., Alonso-Herrero et al.

¹⁰ Another commonly used definition of L_{IR} is the total luminosity from 1–1000 μm . This will differ from $L_{8-1000\mu\text{m}}$ by only a few percent, and for the remaining analysis, we take $L_{\text{IR}} \equiv L_{8-1000\mu\text{m}}$, as defined by Sanders & Mirabel (1996).

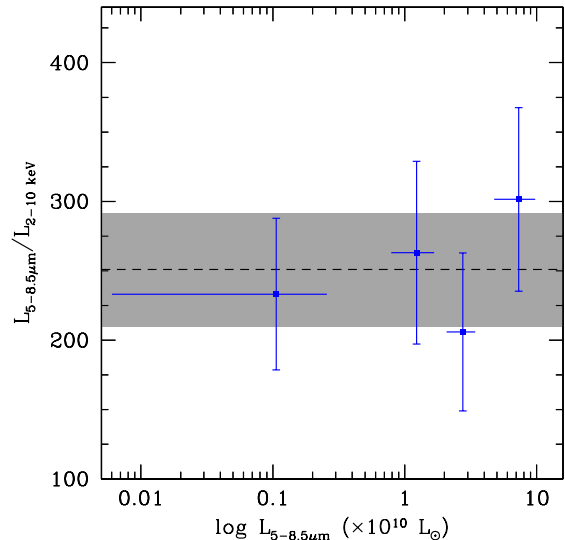


FIG. 4.— Ratio of $L_{5-8.5\mu\text{m}}$ and stacked rest-frame 2–10 keV X-ray luminosity in bins of $L_{5-8.5\mu\text{m}}$ for galaxies with redshifts $1.5 < z < 2.6$ and those with inferred ages greater than 100 Myr. We have excluded sources directly-detected in the *Chandra* 2 Ms data. The faintest bin is for galaxies undetected at $24 \mu\text{m}$. Horizontal error bars indicate the 1σ dispersion in $L_{5-8.5\mu\text{m}}$ in each bin. Vertical error bars show the uncertainty in the mid-IR-to-X-ray luminosity ratio, computed as the uncertainty in the mean X-ray luminosity added in quadrature with the Poisson error in the mean mid-IR luminosity of galaxies in each bin. The dashed horizontal line and shaded region indicate the mean and 1σ uncertainty of the mid-IR-to-X-ray luminosity ratio of $\sim 251 \pm 41$.

2004; Helou et al. 2001; Dale et al. 2001; Normand et al. 1995). Metallicity effects and a changing distribution of dust with respect to HII regions also likely contribute to the observed factor of 2–3 dispersion in the IR/MIR ratios. Nonetheless, the mean IR/MIR flux ratio is similar to that inferred from the Dale et al. (2001) template SED for a median $\log[f_{\nu}(60\mu\text{m})/f_{\nu}(100\mu\text{m})] \sim -0.20$. Based on the sample of 149 galaxies from Elbaz et al. (2002), we assume $L_{\text{IR}} \approx 17.2 L_{5-8.5\mu\text{m}}$ to convert $L_{5-8.5\mu\text{m}}$ to L_{IR} .

It is worth noting that the relationship between $L_{5-8.5\mu\text{m}}$ and total IR luminosity for *local* star-forming galaxies may be described by a more complicated function, such as a two power-law fit (e.g., Elbaz et al. 2002). These complicated relationships may not apply to galaxies at $z \sim 2$ for several reasons. First, the IR/MIR ratio may change depending on the relative contribution of older stellar populations in heating PAH and larger dust grains. The heating of dust by cooler stars is expected to be more prevalent for the less luminous local galaxies with older stellar populations, on average, than for $z \sim 2$ galaxies with relatively younger stellar populations. Second, it is found that $z \sim 2$ galaxies have metallicities that are on average 0.3 dex lower than those of local galaxies at a given stellar mass (Erb et al. 2006a). Therefore, the metallicity dependence of the IR/MIR ratio found for local galaxies (e.g., Engelbracht et al. 2005) suggests that we may not be able to ascribe the IR/MIR ratio for a galaxy of a given stellar mass at $z = 0$ to a galaxy at $z \sim 2$ with the same stellar mass. A third possibility, and one that is suggested by the results of this paper and other studies (e.g., Adelberger & Steidel 2000; Calzetti & Heckman 1999), is that the dust obscuration of galaxies at a given bolometric luminosity changes as

function of redshift, a result that may reflect dust enrichment and/or a changing configuration of dust as galaxies age. Therefore, the relative distribution of PAH and larger dust grains within galaxies may also change as a function of redshift. Because of these uncertainties, and since the primary motivation of our study is to *independently* establish the validity of MIPS observations to infer the infrared luminosities of $z \sim 2$ galaxies, we adopted the simplest conversion that assumes only that the typical IR/MIR luminosity ratio for local galaxies with a wide range in infrared luminosity applies at $z \sim 2$. By taking an average over the local galaxies, we ensure that the derived L_{IR} is not more than a factor of 2–3 away from that predicted using the IR/MIR ratio of any individual galaxy. As we show below, our constant conversion reproduces within the uncertainties the results that we obtain from stacked X-ray and dust-corrected UV estimates of L_{IR} .

In addition to the stacked X-ray and dust-corrected UV estimates, we also have spectroscopic $\text{H}\alpha$ observations for a small sample of 10 $U_n\text{GR}$ galaxies in the GOODS-North field (Erb et al. 2006c) with clean (i.e., not blended) MIPS detections. Once corrected for extinction, the $\text{H}\alpha$ fluxes of these galaxies provide estimates of their total (bolometric) luminosities, which we take to be the sum of the L_{IR} and observed 1600 Å luminosity (uncorrected for extinction):

$$L_{\text{bol}} \equiv L_{\text{IR}} + L_{1600}. \quad (2)$$

In Figure 5 we show the comparison between L_{bol} estimated from the sum of the MIPS-inferred L_{IR} and observed 1600 Å luminosity ($L_{\text{bol}}^{\text{IR}+\text{UV}}$) with L_{bol} estimated from the spectroscopic $\text{H}\alpha$ observations ($L_{\text{bol}}^{\text{H}\alpha}$). The results indicate that within the uncertainties the two estimates of L_{bol} track each other very well (with a scatter of 0.2 dex) over the range of L_{bol} typical of galaxies in optical/near-IR selected samples (§ 7), at least for this limited sample of 10 objects. The agreement between the MIPS and $\text{H}\alpha$ -inferred estimates suggests that our conversion relation between $L_{5-8.5\mu\text{m}}$ and L_{IR} works reasonably well. Nonetheless, for comparison with our constant conversion relation, we also consider the effect on our results of assuming a two power-law conversion suggested by Elbaz et al. (2002). As we show below, assuming the two power-law conversion does not change the main conclusions of our study.

The far-infrared luminosity (L_{FIR}) is typically defined to be the luminosity from 40–120 μm (Helou et al. 1988). Soifer et al. (1987) found $L_{\text{IR}} \sim (1.91 \pm 0.17) \times L_{\text{FIR}}$ for galaxies in their Bright Galaxy Sample. Modeling of the warm and cool components of the dust emission in UV-bright galaxies indicates a conversion factor of ~ 1.75 (Calzetti et al. 2000). We take a median value of ~ 1.80 in converting the inferred L_{IR} of galaxies to a FIR luminosity. Generally, uncertainties in the conversion between L_{IR} and L_{FIR} are much smaller than the uncertainties in converting $L_{5-8.5\mu\text{m}}$ to L_{IR} .

Hereafter we assume uncertainties in the total infrared luminosities as follows. For $U_n\text{GR}$ galaxies and radio-selected SMGs with spectroscopic redshifts, we assume an uncertainty in $\log L_{\text{IR}}$ of 0.3 dex, corresponding to the dispersion in the conversion between $L_{5-8.5\mu\text{m}}$ and L_{IR} . For near-IR selected BzK galaxies and DRGs, the photometric redshift error will add an additional 0.5 dex

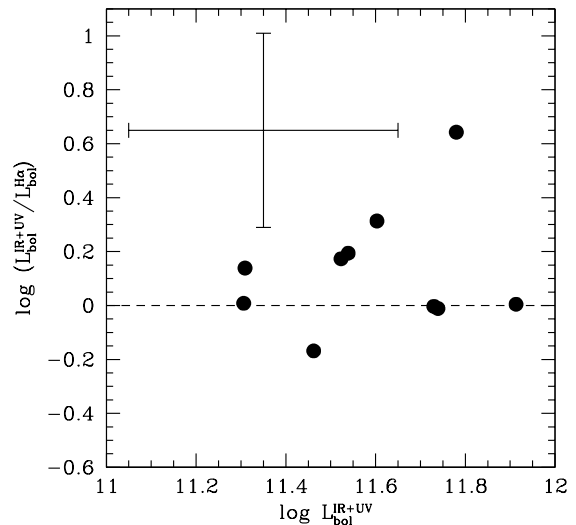


FIG. 5.— Comparison between MIPS-inferred $L_{\text{bol}}^{\text{IR}+\text{UV}}$ and $\text{H}\alpha$ -inferred $L_{\text{bol}}^{\text{H}\alpha}$ for a sample of 10 $U_n\text{GR}$ galaxies. The dispersion in the ratio of the two estimates is ~ 0.2 dex for the subsample considered here. The errorbar shows the typical uncertainty of each point.

scatter. The total uncertainty in $\log L_{\text{IR}}$ for BzK galaxies and DRGs with photometric redshifts is 0.6 dex.

5.2. Infrared Luminosity Distributions

Figure 2 summarizes the observed $f_{24\mu\text{m}}$ fluxes of galaxies as a function of redshift. In this figure, all direct X-ray detections were removed from the $U_n\text{GR}$, BzK and DRG samples, unless they happened to coincide with a radio-detected submillimeter galaxy (SMG) from Chapman et al. (2005), or unless they have spectroscopic redshifts in the $U_n\text{GR}$ sample (crosses in Figure 2). The $U_n\text{GR}$ and SMG samples include objects outside the region covered by our near-IR imaging. The overlap between the samples considered here is discussed extensively in Reddy et al. (2005). The observed 24 μm fluxes for objects in the various samples generally span a large range, from our sensitivity limit of $\sim 8 \mu\text{Jy}$ to $\gtrsim 200 \mu\text{Jy}$.

For a more meaningful comparison, we have computed L_{IR} for galaxies using the prescription described in § 5.1. Figure 6 shows the distribution of L_{IR} as inferred from $L_{5-8.5\mu\text{m}}$ for galaxies in the $U_n\text{GR}$, BzK/SF , DRG, and radio-detected SMG (Chapman et al. 2005) samples with either spectroscopic or photometric redshifts $1.5 < z < 2.6$. As in Figure 2, we have excluded directly detected X-ray sources from the distributions unless they coincide with a radio-detected SMG source. We show the resulting distributions assuming the constant conversion and two power-law conversion relations in the left and right panels, respectively. The distributions assuming the two power-law conversion are bimodal. However, the distributions of observed UV luminosities and dust correction factors of $U_n\text{GR}$ galaxies are approximately gaussian (e.g., Steidel et al. 2004; Reddy et al. 2006). Assuming the Calzetti et al. (2000) law to convert the observed luminosities to dust-corrected luminosities then implies that the bolometric luminosity distribution of $U_n\text{GR}$ galaxies should be gaussian, a result not in accordance with the bimodal distribution computed assuming the two power-law conversion. More generally, we expect

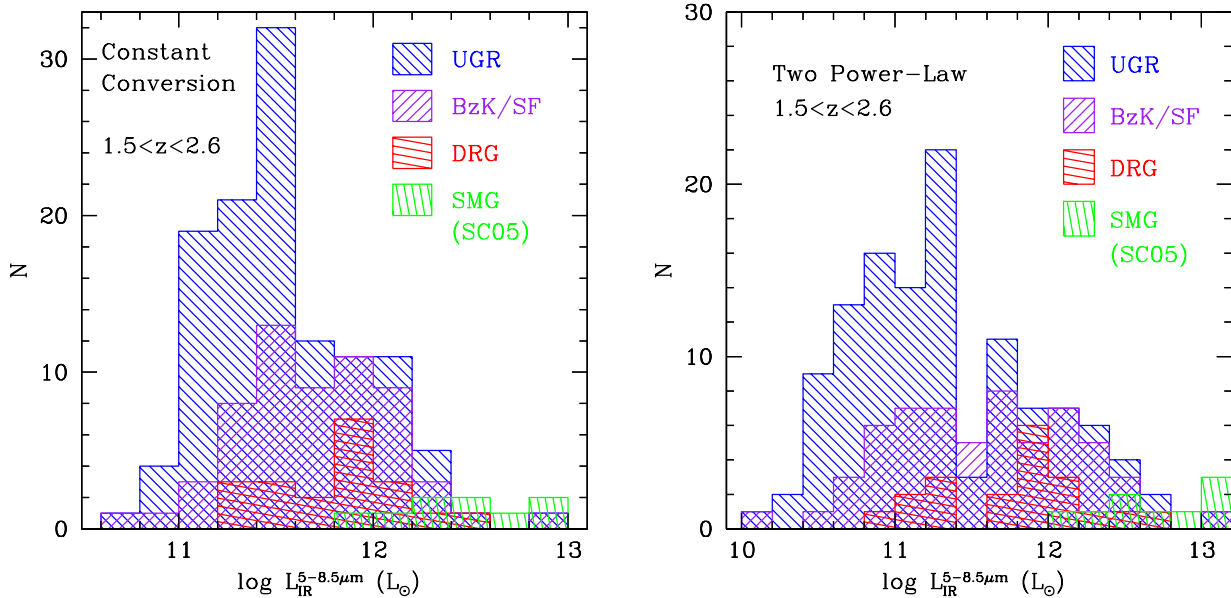


FIG. 6.— Distributions of L_{IR} as inferred from $L_{5-8.5\mu\text{m}}$ for galaxies in the U_nGR , BzK/SF , DRG, and radio-detected SMG (Chapman et al. 2005) samples with redshifts $1.5 < z < 2.6$ assuming our constant conversion between $L_{5-8.5\mu\text{m}}$ and L_{IR} (left panel) and the two power-law conversion of Elbaz et al. (2002) (right panel). We have excluded directly-detected X-ray sources unless they happen to coincide with a radio-detected SMG.

to find gaussian distributions of luminosity for galaxies in photometric surveys since such galaxies are typically selected on a continuous range of observed colors and/or magnitudes. The bimodality in Figure 6b is likely due to the sparse data used to establish the two power-law relation for galaxies with $1 \times 10^{11} \lesssim L_{\text{IR}} \lesssim 5 \times 10^{11} L_{\odot}$ (see Figure 5d of Elbaz et al. 2002). This range of L_{IR} happens to encompass the typical IR luminosity of $z \sim 2$ galaxies as inferred from X-ray and dust-corrected UV estimates (Reddy & Steidel 2004) and it is partly for this reason that we favored our simple constant conversion relationship.

Regardless of the conversion used, we find that the bulk of the galaxies in the U_nGR and BzK/SF samples and detected at $24 \mu\text{m}$ have inferred infrared luminosities comparable to those of local luminous infrared galaxies (LIRGs), with $10^{11} \lesssim L_{\text{IR}} \lesssim 10^{12} L_{\odot}$. Galaxies in the U_nGR sample with $f_{24\mu\text{m}} \gtrsim 8 \mu\text{Jy}$ (corresponding to the 3σ sensitivity limit) have $\langle L_{\text{IR}} \rangle \sim 3.1 \times 10^{11} L_{\odot}$ for the constant conversion and $\langle L_{\text{IR}} \rangle \sim 2.1 \times 10^{11} L_{\odot}$ for the two power-law conversion (the two power-law distribution is broader than that obtained using the constant conversion). Both the U_nGR and BzK/SF samples also host galaxies which, based on their inferred L_{IR} , would be considered ultra-luminous infrared galaxies (ULIRGs) with $L_{\text{IR}} \gtrsim 10^{12} L_{\odot}$. Note that if we excluded all direct X-ray detections, including the submillimeter sources, the maximum inferred L_{IR} of U_nGR and BzK/SF galaxies is $\approx 2.5 \times 10^{12} L_{\odot}$, an infrared luminosity which is similar to the detection limit of the *Chandra* 2 Ms data for a galaxy at $z \sim 2$ assuming the Ranalli et al. (2003) conversion between X-ray and FIR luminosity.

The BzK/SF sample distribution shown in Figure 6 includes galaxies that do not satisfy the U_nGR criteria (i.e., $BzK/SF-U_nGR$ galaxies). These galaxies (to $K_s = 21$) have a mean IR luminosity that is identical to that of U_nGR galaxies to $K_s = 21$. The average IR luminosity of U_nGR galaxies is ~ 1.8 times fainter than BzK galaxies

since the U_nGR sample includes galaxies which extend to fainter K_s magnitudes than those in the BzK sample. Therefore, while the $BzK/SF-U_nGR$ galaxies have redder $G-R$ colors than required to satisfy the U_nGR criteria, it appears that their infrared luminosities are still comparable to those of U_nGR galaxies (see also the discussion in § 6), a result consistent with that obtained in X-ray stacking analyses (Reddy et al. 2005). Figure 6 indicates the DRG galaxies with photometric redshifts between $1.5 < z < 2.6$ also span a large range in L_{IR} , from luminosities characteristic of LIRGs to ULIRGs. We find a luminosity distribution of DRGs to $K_s = 21$ that is in good agreement with the L_{IR} distribution found by Papovich et al. (2005) for DRGs (to approximately the same depth) in the GOODS-South field¹¹. We note that U_nGR galaxies and DRGs to $K_s = 20$ have the same inferred L_{IR} as $K_s < 20$ galaxies selected in other ways (e.g., using the BzK/SF criteria).

The inferred L_{IR} for the one BzK/PE selected galaxy with $z \sim 1.5$ is $\sim 1.2 \times 10^{12} L_{\odot}$. The mean $f_{24\mu\text{m}}$ flux of MIPS-detected (and non X-ray detected) BzK/PE galaxies without redshifts is $\langle f_{24\mu\text{m}} \rangle \approx 81.4 \mu\text{Jy}$ which, at the mean redshift of BzK/PE galaxies (e.g., Reddy et al. 2005; Daddi et al. 2004) of $z \sim 1.7$, corresponds to $L_{\text{IR}} \sim 6 \times 10^{11} L_{\odot}$. The $24 \mu\text{m}$ detection rate ($\sim 50\%$; Table 1) of non X-ray detected BzK/PE galaxies implies some contamination by star-forming galaxies; this is not unexpected given that photometric scattering can have a significant effect on samples constructed by color selection techniques (Reddy et al. 2005).

The radio-detected submillimeter galaxies to $S_{850\mu\text{m}} \sim 4.2 \text{ mJy}$ analyzed here have inferred L_{IR} of $10^{12} \lesssim L_{\text{IR}} \lesssim 10^{13} L_{\odot}$, which can be directly compared with their bolometric luminosities calculated based on the submillimeter data presented by Chapman et al. (2005). The

¹¹ The DRG sample of Papovich et al. (2005) extends to $K_s = 23.2$ in AB magnitudes, or $K_s \sim 21.4$ in Vega magnitudes, over an area twice as large as studied here.

850 μm -inferred bolometric luminosities ($L_{\text{IR}}^{850\mu\text{m}}$) are sensitive to the assumed characteristic dust temperature associated with a greybody fit to the dust SED and the emissivity. For example, a change in the assumed dust temperature from $T_d = 36$ K (the median value for the sample of radio-detected SMGs in Chapman et al. 2005) to a cooler temperature of $T_d = 31$ K results in a factor of ~ 5 decrease in the inferred FIR luminosities. Figure 7 shows the comparison between 850 μm and 24 μm inferred bolometric luminosities of radio-detected SMGs. We also show the point corresponding to IRS9 from the Yan et al. (2005) sample of hyperluminous $z = 2$ sources with IRS spectroscopy — this source has independent constraints on its FIR luminosity based on MIPS 70 and 160 μm and MAMBO millimeter measurements. The infrared luminosity of IRS9 is $L_{\text{IR}} \sim 1.8 \times 10^{13} L_{\odot}$ (constrained to within a factor of 2–3) based on these multi-wavelength measurements (Yan et al. 2005).

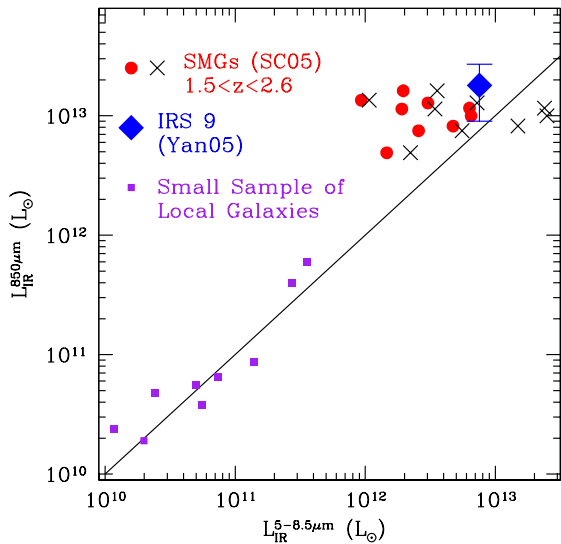


FIG. 7.— $L_{\text{IR}}^{850\mu\text{m}}$, inferred from the submillimeter fluxes of radio-detected SMGs (Chapman et al. 2005), plotted against $L_{\text{IR}}^{5-8.5\mu\text{m}}$ inferred from $L_{5-8.5\mu\text{m}}$ assuming a IR/MIR flux conversion of 17.2 (solid circles) and the two power-law conversion of Elbaz et al. (2002) (crosses). The infrared luminosity of IRS9 is inferred from MIPS 24, 70, and 160 μm data and MAMBO millimeter measurements (Yan et al. 2005). Also shown are the local star-forming templates listed in Table 2.

Figure 7 shows that the IR/MIR flux ratio for IRS9 is comparable (to within $\sim 1 \sigma$) to those of the local star-forming galaxies listed in Table 2— these local galaxies are 1–3 orders of magnitude fainter than IRS9. Judging the validity of our conversion for the hyper-luminous galaxies at $z \sim 2$ is difficult given that very few of these galaxies have independent constraints on their bolometric luminosities. On the other hand, the submillimeter (850 μm) inferred infrared luminosities of bright SMGs are systematically a factor of 2–10 higher than predicted using our conversion between $L_{5-8.5\mu\text{m}}$ and L_{IR} . The crosses in Figure 7 demonstrate that the systematic offset cannot be completely accounted for if we assume a two power-law conversion between $L_{5-8.5\mu\text{m}}$ and L_{IR} — there are still 4 of 9 SMGs with $L_{\text{IR}}^{850\mu\text{m}}$ that are factor of 2–10 larger than predicted from their 24 μm fluxes, and the distribution of SMG points when con-

sidering the two-power law conversion is not symmetric about the line of equality (solid line in Figure 7). One possibility is that the submillimeter estimates are in fact correct and that our assumed conversion between mid-IR and IR luminosities does not apply to SMGs. The IRS sample considered here consists of just one hyperluminous galaxy at $z = 2$, and if we ignore this galaxy then the systematic offset of SMGs may indicate a breakdown of our assumed conversion for the most luminous sources at redshifts $z \sim 2$ with $L_{\text{IR}} \gtrsim 10^{13} L_{\odot}$. The second possibility is that the submillimeter estimates over-predict the infrared luminosities of SMGs and that our MIR-to-IR conversion is correct. This may not be surprising since the conversion between submillimeter flux and bolometric luminosity is very sensitive to the assumed dust temperature, and a decrease in the assumed temperature of just a few degrees can reduce the inferred bolometric luminosity by a factor of $\sim 5 - 10$ (see example above). Finally, it is possible that neither the submillimeter or mid-IR inferred infrared luminosities of bright SMGs is correct. We note that it is common for these luminous galaxies to host AGN, and this can alter the observed mid-IR and IR fluxes beyond what would be expected given pure star formation (e.g., Armus et al. 2004; Fadda et al. 2002; Almaini et al. 1999; Fabian & Iwasawa 1999). As another example, Arp 220 has anomalously low PAH emission for its bolometric luminosity (when compared with other ULIRGs), suggesting that the galaxy contains a buried quasar and/or a heavily dust-enshrouded starburst such that the extinction at rest-frame 7 μm is no longer negligible (e.g., Haas et al. 2001; Charmandaris et al. 1997). *Spitzer* IRS observations of bright radio-detected SMGs will be useful in quantifying the relationship between the 5–8.5 μm and bolometric luminosities of these ultraluminous sources.

A relevant line of investigation is to determine what the various optical and near-IR color and magnitude selections imply for the infrared luminosity distributions of the galaxies they select. Figure 8a shows the inferred L_{IR} of galaxies with redshifts $1.5 < z < 2.6$ as a function of K_s magnitude. We have assumed the IR/MIR flux ratio of 17.2 for the radio-detected SMGs shown in the figure. Galaxies with $K_s < 20$ (e.g., K20 samples: Cimatti et al. 2002a; Cimatti et al. 2002b) have $\langle L_{\text{IR}} \rangle \sim (1 - 2) \times 10^{12} L_{\odot}$, similar to the value found by Daddi et al. (2005) for $K_s < 20$ *BzK* selected galaxies in the GOODS-N field. Alternatively, we find $\langle L_{\text{IR}} \rangle \sim 5 \times 10^{11} L_{\odot}$ for *U_nGR*, *BzK*, and DRG galaxies with $20 < K_s < 21.0$. As stated in § 5.1, the uncertainties on any individual value of $\log L_{\text{IR}}$ are 0.3 dex for *U_nGR* galaxies with spectroscopic redshifts and 0.6 dex for near-IR selected (*BzK*; DRG) galaxies with photometric redshifts. At any given K_s magnitude, the range in L_{IR} spans an order of magnitude assuming our constant conversion and larger than an order of magnitude assuming the two power-law conversion of Elbaz et al. (2002). Finally we note that galaxies with $K_s < 20$ at $z \sim 2$ which show some signature of star formation (i.e., those that are MIPS detected) generally have infrared luminosities that are a factor of two larger than those of galaxies with $20 < K_s < 21$. As discussed elsewhere, there is also a population of massive galaxies with little detectable star formation (e.g., van Dokkum et al. 2004;

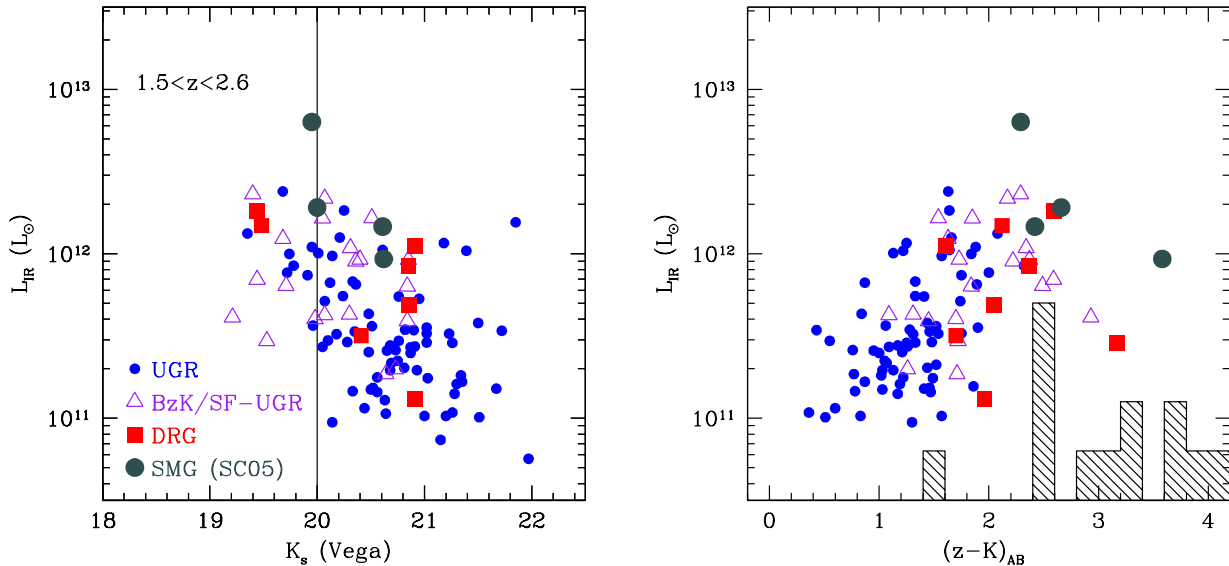


FIG. 8.— *Left panel:* Distribution of L_{IR} as a function of K_s for galaxies in the various samples. We have assumed a IR/MIR flux ratio of 17.2 for all galaxies including the radio-detected SMGs. *Right panel:* L_{IR} as a function of $(z - K)_{\text{AB}}$ color. Symbols are the same as in the left panel. The arbitrarily normalized histogram indicates the distribution in $(z - K)_{\text{AB}}$ color of DRGs and BzK/PE galaxies undetected at $24 \mu\text{m}$.

Reddy et al. 2005).

We investigate this quiescent population of massive galaxies in the context of their star-forming counterparts by examining L_{IR} as a function of $(z - K)_{\text{AB}}$ color (Figure 8b). The $(z - K)_{\text{AB}}$ color probes the Balmer and 4000 \AA breaks for galaxies at the redshifts of interest here, and is also sensitive to the current star formation rate (e.g., Reddy et al. 2005; Daddi et al. 2004). Figure 8b shows that galaxies with redder $(z - K)_{\text{AB}}$ color (up to $(z - K)_{\text{AB}} \sim 3$) have higher inferred L_{IR} (and larger SFRs if the bolometric luminosity is attributed to star formation) on average than galaxies with bluer $(z - K)_{\text{AB}}$ colors, a trend similar to that found when stacking X-ray data (Reddy et al. 2005). A more interesting result is indicated by the histogram which shows the distribution in $(z - K)_{\text{AB}}$ color of DRGs and BzK/PE galaxies that are undetected at $24 \mu\text{m}$. Of the 13 MIPS-undetected DRGs and BzK/PE galaxies, 7 have $(z - K)_{\text{AB}} > 3$. Reddy et al. (2005) found DRGs with $(z - K)_{\text{AB}} \gtrsim 3$ to have little X-ray emission and had colors similar to those of IRAC Extremely Red Objects (IEROs; Yan et al. 2005). The lack of $24 \mu\text{m}$ detections for these red $(z - K)_{\text{AB}}$ sources further supports the notion that they have little current star formation. It also rules out the possibility that they harbor Compton-thick obscured AGN as an explanation for their lack of X-ray emission, since we would then expect them to be bright at $24 \mu\text{m}$.

5.3. Stacked $24 \mu\text{m}$ Flux

The high quality and depth of the MIPS data enable us to study the average properties of galaxies that are (individually) undetected at $24 \mu\text{m}$ by stacking their emission. The data were stacked by considering all galaxies undetected at $24 \mu\text{m}$ and X-ray wavelengths. To avoid contaminating the stacked signal, we only added galaxies to the stack if there were no bright MIPS sources within $\approx 5''$ of those galaxies. To ensure a clean signal, we extracted sub-images around each un-

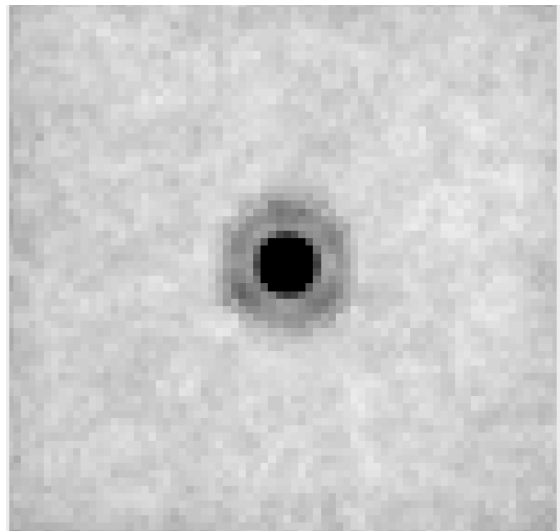


FIG. 9.— Stacked $24 \mu\text{m}$ flux of 48 isolated MIPS-undetected U_nGR galaxies ($f_{24\mu\text{m}} \lesssim 8 \mu\text{Jy}$) with spectroscopic redshifts $1.5 < z < 2.6$, indicating a mean flux per undetected galaxy of $\langle f_{24\mu\text{m}} \rangle \approx 3.30 \pm 0.48 \mu\text{Jy}$.

detected galaxy, subtracted all *detected* point sources within those sub-images using the empirical PSF, and added the sub-images together. The stacked flux was measured in a manner similar to the measurement of detected MIPS sources. Figure 9 shows the stacked image of 48 MIPS-undetected U_nGR galaxies with spectroscopic redshifts $1.5 < z < 2.6$. The mean flux per object is $\langle f_{24\mu\text{m}} \rangle \approx 3.30 \pm 0.48 \mu\text{Jy}$, where the error is the dispersion of the background in the *stacked* image. At a mean redshift of $\langle z \rangle = 2.05$, this flux corresponds to $L_{\text{IR}} \approx 2 \times 10^{10} L_{\odot}$. Combining this result with the mean L_{IR} of MIPS-detected U_nGR galaxies implies a mean across the entire sample, neglecting “confused” sources, of $\approx 2.3 \times 10^{11} L_{\odot}$. This mean value does not change significantly if we add in directly-detected X-ray sources (including radio-detected SMGs

to $S_{850\mu\text{m}} \sim 5$ mJy) because of their small number compared to the typical (less luminous) U_nGR galaxy. The mean value of $L_{\text{IR}} \approx 2.3 \times 10^{11} L_{\odot}$ is in excellent agreement with the average of $L_{\text{IR}} \approx 3 \times 10^{11} L_{\odot}$ found from stacked X-ray/radio and dust corrected UV estimates (Reddy & Steidel 2004). This suggests that the non-detection of galaxies at $24 \mu\text{m}$ is due to them having lower SFRs and not because they are deficient in PAH emission for a given L_{IR} . The advantage of the $24 \mu\text{m}$ data over X-ray/radio data is that we can estimate bolometric luminosities for individual L^* (LIRG) galaxies at $z \sim 2$ rather than ensembles of galaxies.

Combining our estimate of the MIPS-inferred average IR luminosity of U_nGR galaxies with the stacked radio results of Reddy & Steidel (2004), we find that the radio-IR relation appears valid on average for the sample. To quantify the radio-IR ratio for the sample, we compute the “q” parameter (Condon et al. 1991):

$$q \equiv \log\left(\frac{\text{FIR}}{3.75 \times 10^{12} \text{ W m}^{-2}}\right) - \log\left(\frac{S_{1.4 \text{ GHz}}}{\text{W m}^{-2} \text{ Hz}^{-1}}\right), (3)$$

where $S_{1.4 \text{ GHz}}$ is the rest-frame 1.4 GHz flux density in units of $\text{W m}^{-2} \text{ Hz}^{-1}$ and

$$\text{FIR} \equiv 1.26 \times 10^{-14} (2.58 S_{60 \mu\text{m}} + S_{100 \mu\text{m}}) \text{ W m}^{-2}, (4)$$

where $S_{60 \mu\text{m}}$ and $S_{100 \mu\text{m}}$ are the IRAS 60 and 100 μm flux densities in Jy (Helou et al. 1988). The implied “q” value for the U_nGR sample is $\langle q \rangle \sim 2.5$ if we assume $\log[S_{60 \mu\text{m}}/S_{100 \mu\text{m}}] \sim 0.2$. This value of q is in excellent agreement with the value of $q \sim 2.4$ found for $\gtrsim 10^{11} L_{\odot}$ galaxies in the IRAS 2 Jy sample (Yun et al. 2001). We also stacked the $24 \mu\text{m}$ data for undetected BzK/PE and DRG galaxies in the same manner as described above, which yielded a mean flux per object of $\langle f_{24\mu\text{m}} \rangle \sim 2.72 \pm 1.65 \mu\text{Jy}$. As noted in § 5.2, most of these sources have very red $(z-K)_{\text{AB}}$ colors, and their low-level mid-IR and X-ray emission indicate they have low SFRs. Galaxies with $f_{24\mu\text{m}} \lesssim 8 \mu\text{Jy}$ are discussed further below.

6. DUST ATTENUATION IN OPTICAL AND NEAR-IR SELECTED GALAXIES

Aside from inferring the infrared luminosity distributions, we can use the MIPS data to examine the relationship between dust extinction and rest-frame UV spectral slope. Meurer et al. (1999) found a relation between the rest-frame UV spectral slope, β , and the attenuation of local UV-selected starburst galaxies, parameterized by the ratio L_{FIR}/L_{1600} , where L_{1600} is the rest-frame 1600 Å luminosity uncorrected for extinction. This relation appears to fail, however, for the most luminous starbursts such as ULIRGs (Goldader et al. 2002) and radio-detected SMGs (Chapman et al. 2005). A greater proportion of the star formation in galaxies with $L_{\text{IR}} \gtrsim 10^{12} L_{\odot}$ will be obscured by dust as compared with LIRG-type starbursts (e.g., see § 7). Therefore, whatever UV emission is able to escape from the optically-thin regions of ULIRGs will constitute a lower fraction of the total bolometric luminosity. As a result, the rest-frame UV light can substantially underpredict (by a factor of 10–100) the bolometric luminosities of the most luminous starbursts, such as radio-detected SMGs (Chapman et al. 2005). Normal (“quiescent”) star forming galaxies also appear to deviate from the Meurer et al. (1999) relation, such that L_{FIR}/L_{1600} is lower for a given

amount of UV reddening than in starburst galaxies (e.g., Laird et al. 2005; Bell 2002) a result that may be tied to the varying ratio of current to past-average star formation rate of normal star forming galaxies (Kong et al. 2004). Alternatively, the star formation in local quiescent galaxies (i.e., those with low SFRs) is more distributed than in local starbursts so that a failure of the starburst reddening law may reflect a different distribution of dust with respect to the star forming regions in quiescent galaxies. Observations of radio-detected SMGs and quiescently star-forming galaxies suggests that the Meurer et al. (1999) and Calzetti et al. (2000) laws do not apply to these sources.

The rest-frame UV spectral and mid-IR data of $z \sim 2$ galaxies allow us to investigate how well the high redshift galaxies follow the local dust attenuation relation. The full SED modeling of U_nGR galaxies in the GOODS-N field yields estimates of the best-fit star formation history (τ), age, mass, SFR, and $E(B-V)$ color excess for each galaxy (Erb et al. 2006b; Shapley et al. 2005). The mean fractional uncertainty in $E(B-V)$ is $\langle \sigma_{E(B-V)} \rangle / E(B-V) = 0.7$ as determined from Monte Carlo simulations. To convert $E(B-V)$ to β we assumed that 1 mag of extinction at 1600 Å ($A_{1600} = 1$) corresponds to $E(B-V) \approx 0.092$ (e.g., Calzetti et al. 2000). For most galaxies, the best-fit star formation history is close to that of a constant star formation history (with decay time-scale $\tau = \infty$). The most massive galaxies at $z \sim 2$ (with stellar masses $M^* \gtrsim 10^{11} M_{\odot}$) are generally better fit with declining star formation histories. We have assumed a CSF model for galaxies unless such a model provides a much poorer fit to the observed data than a declining star formation history.

6.1. Results for Optically Selected Galaxies

Figure 10 shows L_{FIR}/L_{1600} versus β for spectroscopically-confirmed U_nGR galaxies with redshifts $1.5 < z < 2.6$. The FIR luminosity is computed from $L_{5-8.5\mu\text{m}}$ using the procedure described in § 5.1. We estimated the rest-frame 1600 Å luminosity from either the U_n , G , or R magnitude depending on the redshift of the galaxy. The majority of U_nGR galaxies with inferred ages $\gtrsim 100$ Myr (solid circles) appear to agree well with Meurer et al. (1999) relation, shown by the solid curve¹².

U_nGR galaxies with the youngest inferred ages ($\lesssim 100$ Myr; open circles) exhibit a large offset from the Meurer et al. (1999) relation in the sense that they exhibit redder UV colors for a given dust obscuration than older galaxies which do follow the relation. Note that we have assumed a CSF model for the young galaxies shown in Figure 10. The inferred ages of these galaxies are typically smaller than 50 Myr, which is approximately the dynamical time across the galaxy. Assuming such small (and unrealistic ages) will cause us to overestimate $E(B-V)$ for these sources. The change in $E(B-V)$ that results from fixing the age of the young galaxies to 100 Myr ($\Delta E(B-V) = 0.09$) is not enough to completely account for the offset of the young galaxies from the Meurer et al. (1999) relation. This suggests

¹² Assuming the two power-law conversion to compute L_{FIR} results in a similar distribution of points around the Meurer et al. (1999) relation but with larger scatter.

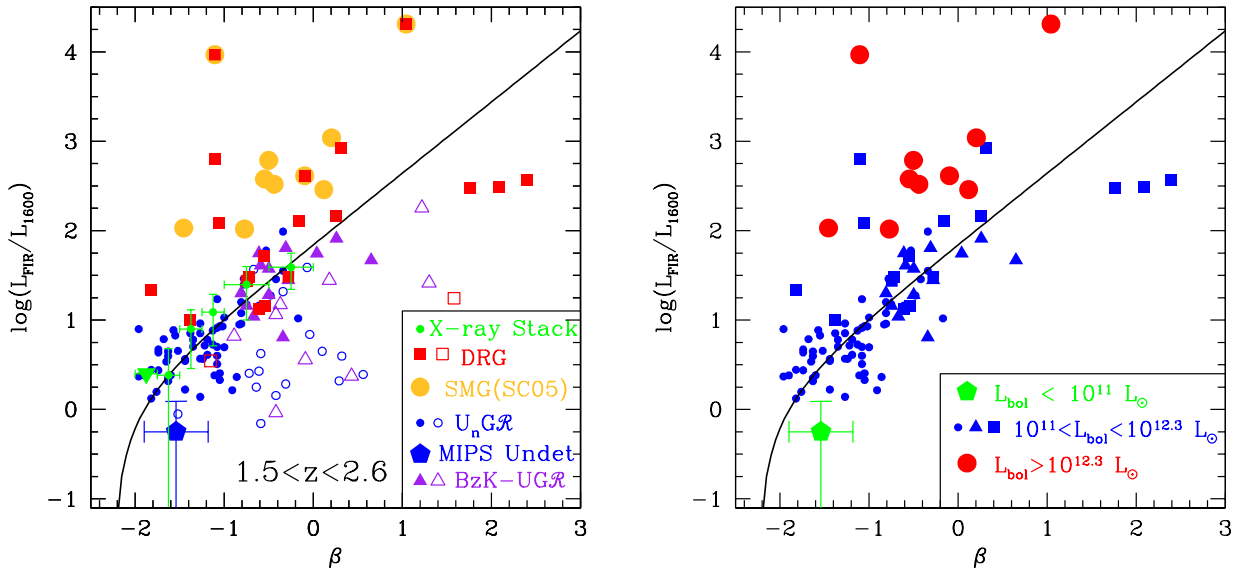


FIG. 10.— (*Left*) Dust absorption, parameterized by F_{FIR}/F_{1600} , versus rest-frame UV spectral slope, β , for galaxies with redshifts $1.5 < z < 2.6$. Filled and open symbols respectively denote galaxies with inferred ages of > 100 Myr and < 100 Myr. The large pentagon shows the results for U_nGR galaxies undetected at $24 \mu\text{m}$, using the stacked results of § 5.3. The horizontal and vertical error bars on this point reflect the dispersion about the mean β and mean L_{FIR}/L_{1600} of $24 \mu\text{m}$ undetected sources. The green points represent the results from an X-ray stacking analysis as described in the text. The solid line indicates the Meurer et al. (1999) relation found for local UV-selected starburst galaxies. (*Right*) Same as *left* panel, but excluding galaxies younger than 100 Myr and color-coding objects by L_{bol} .

that Calzetti et al. (2000) law may not be applicable to these young galaxies because of a different configuration of dust with respect to the star-forming regions, in which case a grayer extinction law may be appropriate. As one example, the well-studied lensed Lyman Break Galaxy MS1512-cB58 has an inferred age of $\sim 70 - 100$ Myr and millimeter continuum observations suggest that its infrared luminosity is smaller than one would predict from its UV reddening (Baker et al. 2001). Regardless of the assumed extinction law, these young galaxies in the samples examined here have similar bolometric (sum of observed IR and UV) luminosities as older galaxies (see § 7).

The deep X-ray data in the GOODS-N field allow us to estimate (X-ray inferred) average infrared luminosities for well-defined samples of galaxies (e.g., Reddy et al. 2005; Laird et al. 2005; Nandra et al. 2002; Brandt et al. 2001). The green points in Figure 10 show the expected dust absorption inferred from the X-ray data as a function of β . These points were determined by stacking the X-ray data for non X-ray detected U_nGR galaxies (with ages > 100 Myr) in bins of β . We only considered stacking galaxies with ages > 100 Myr since the X-ray emission is sensitive to the star formation rate once O and B stars evolve to produce high mass X-ray binaries, which is roughly 10^8 years after the onset of star formation. The average X-ray flux per bin was converted to a FIR flux using the Ranalli et al. (2003) relation. Dividing the average FIR flux per bin by the average 1600 \AA luminosity of objects in each bin yields the green points. The horizontal error bars indicate the bin width and the vertical error bars indicate the dispersion in stacked X-ray flux (computed using the procedure described in Reddy et al. (2005) and Reddy & Steidel (2004)) added in quadrature with the dispersion in the FIR/X-ray luminosity relation found by Ranalli et al. (2003). The X-ray results reproduce the Meurer et al. (1999) relation very well, providing an independent confirmation that typical U_nGR

galaxies abide by the local dust obscuration relation for starburst galaxies. The X-ray and mid-IR data indicate that the UV slope can be used to deduce the extinction corrections for these typical galaxies and that such galaxies have UV light that is only moderately extinguished in most cases. The agreement between the MIPS inferred FIR luminosities and X-ray inferred FIR luminosities (obtained with the empirically-determined Ranalli et al. (2003) relation) suggests that the Ranalli et al. (2003) relation provides a reasonable description for most of the galaxies considered here. For comparison, adopting the Persic et al. (2004) relation would yield FIR luminosities five times in excess of those predicted from the $24 \mu\text{m}$ fluxes for the vast majority of $z \sim 2$ galaxies.

We compute the average dust obscuration of U_nGR galaxies undetected at $24 \mu\text{m}$ using the stacking results of § 5.3, and the result is denoted by the large pentagon in Figure 10. The stacked $24 \mu\text{m}$ FIR luminosity of MIPS undetected galaxies is divided by their average rest-frame 1600 \AA luminosity. For these galaxies, L_{1600} is on average 1.6 times larger than their inferred L_{FIR} indicating they are significantly less obscured than galaxies detected at $24 \mu\text{m}$. These undetected galaxies also have relatively blue rest-frame UV SEDs (as indicated by their average β) compared to $24 \mu\text{m}$ detected galaxies. Furthermore, the results of Figure 4 indicate these faint sources have lower X-ray emission than $24 \mu\text{m}$ detected galaxies. All of these observations combined suggest that galaxies are undetected at $24 \mu\text{m}$ because they have lower SFRs and are less obscured than galaxies with brighter $24 \mu\text{m}$ fluxes. We further explore the nature of these MIPS undetected sources in § 8.

6.2. Results for Near-IR and Submillimeter Selected Galaxies

Also shown in Figure 10 are BzK/SF galaxies to $K_s = 21$ not satisfying the U_nGR criteria. As pointed out in § 5.2, these BzK/SF selected galaxies have inferred L_{IR}

that are comparable to those of U_nGR galaxies to the same K_s limit, but of course with redder $G - \mathcal{R}$ colors and a $\mathcal{R} \sim 0.5$ mag fainter on average than U_nGR galaxies to the same K_s limit. The results of Figure 10 suggest that BzK/SF galaxies lying outside the color range selected by the U_nGR criteria also follow the Meurer et al. (1999) relation. Similar to the results found in § 6.1 for most U_nGR galaxies, the mid-IR data indicate that the UV light from most BzK/SF galaxies appears to be moderately extinguished and that the UV slope can be used to estimate their attenuation.

Almost all of the radio-detected SMGs considered here have inferred dust absorption factors (when we assume the $850 \mu\text{m}$ -inferred bolometric luminosities) that are at least a magnitude larger than predicted by the Meurer et al. (1999) relation for a given rest-frame UV slope. The discrepancy is not as substantial (i.e., it is reduced by a factor of $2 - 10$) if we inferred L_{IR} of the SMGs from their $24 \mu\text{m}$ fluxes assuming our conversion between MIR and IR luminosity. The U_nGR criteria are designed to select objects where followup spectroscopy is feasible, and this usually implies setting a limit to the allowed $E(B - V)$ (or β) of objects in the sample. However, given that at least half the galaxies with $L_{\text{bol}} \gtrsim 10^{12} L_{\odot}$ have UV slopes comparable to that of the *typical* U_nGR galaxy, it is not uncommon to find such dust-obscured galaxies in optical surveys.

Of the limited sample of DRGs with photometric redshifts $1.5 < z < 2.6$, at least half lie above the local starburst attenuation law. We are able to find DRGs that agree with the Meurer et al. (1999) relation since the MIPS data studied here are significantly deeper (by a factor of ~ 5) than the data considered in Papovich et al. (2005). In particular, we find the surface density of DRGs between $1.5 < z < 2.6$ with $1 \lesssim \log(F_{\text{FIR}}/F_{1600}) \lesssim 2$ of $\gtrsim 0.14 \text{ arcmin}^{-2}$ (this is a lower limit since there are number of DRGs without photometric redshifts, some of which may truly lie at redshifts $1.5 < z < 2.6$), which is at least a factor of 20 higher than in Papovich et al. (2005). Our results suggest that the DRG population consists of galaxies with a very wide range in star formation rate, from galaxies with little or no star formation (DRGs with very red $(z - K)_{\text{AB}}$ colors; § 5.2) to those which are heavily obscured and rapidly forming stars.

6.3. Relationship between β and Obscuration as a Function of Luminosity

Figure 10b shows galaxies with ages > 100 Myr within the samples, color-coded by their L_{bol} . Virtually all objects with L_{bol} in the range $10^{11} < L_{\text{bol}} < 10^{12.3} L_{\odot}$ have β which appear to reproduce their obscuration as inferred from the Meurer et al. (1999) and Calzetti et al. (2000) laws. There is some weaker evidence that the galaxies with the lowest SFRs (undetected at $24 \mu\text{m}$) as indicated by the green pentagon in Figure 10b follow a different extinction law. More pronounced, however, is the systematic offset of the most luminous galaxies considered here with $L_{\text{bol}} > 10^{12.3} L_{\odot}$. These ultraluminous galaxies have rest-frame UV slopes that underpredict their obscuration by a factor of $10 - 100$. The main results of Figure 10b indicate that the relationship between UV reddening and obscuration is strongly dependent on the bolometric luminosity, but that most LIRG galaxies at

$z \sim 2$ follow the local relation.

7. RELATIONSHIP BETWEEN DUST OBSCURATION AND BOLOMETRIC LUMINOSITY

The bolometric luminosity of star-forming galaxies can be well-approximated by the sum of the IR and UV luminosities as indicated in Equation 5. Figure 11 shows L_{bol} as a function of dust obscuration for objects in the various samples assuming a constant conversion relation between mid-IR and total IR luminosity. Typical (LIRG) galaxies at $z \sim 2$ will have $L_{\text{bol}} \approx L_{\text{IR}}$ where $\sim 90\%$ of the bolometric luminosity is emitted in the infrared. The bolometric luminosity is strongly correlated with dust obscuration: galaxies with larger bolometric luminosities are more dust obscured than less luminous galaxies. The best-fit linear trend for spectroscopically-confirmed U_nGR galaxies detected at $24 \mu\text{m}$ is

$$\log L_{\text{bol}} = (0.62 \pm 0.06) \log \frac{L_{\text{IR}}}{L_{1600}} + (10.95 \pm 0.07) \quad (5)$$

(solid line in Figure 11; we note that the two axes are not independent of each and may partly account for the tight scatter in the correlation). U_nGR galaxies undetected at $24 \mu\text{m}$ are indicated by the pentagon. These undetected galaxies have an average bolometric luminosity of $\langle L_{\text{bol}} \rangle \sim 6 \times 10^{10} L_{\odot}$ and have UV luminosities that are a factor of ~ 10 less dust obscured than the typical $24 \mu\text{m}$ detected U_nGR galaxy. Approximately half of the bolometric luminosity of these $24 \mu\text{m}$ undetected galaxies is emitted in the UV. Galaxies with inferred ages < 100 Myr (yellow symbols in Figure 11) have L_{bol} comparable to those of older galaxies at $z \sim 2$, suggesting that these young galaxies have similar IR/MIR ratios as older galaxies. Therefore, the deviation of the young galaxies from the Meurer et al. (1999) law as noted in § 6 suggests that we have over-estimated $E(B - V)$ for these young sources and/or they may follow a steeper (e.g., SMC-like) extinction law.

We note that U_nGR galaxies with $K_s < 21$ have bolometric luminosities and dust obscuration comparable to BzK galaxies to $K_s = 21$ that are not optically selected. This implies that objects missed by optical selection but which appear in the near-IR selected BzK sample are not missed because they are more dust obscured, a result corroborated by X-ray stacking analyses (Reddy et al. 2005). The bright radio-detected SMGs have the highest inferred bolometric luminosities among all galaxies considered here, of order $\sim 10^{13} L_{\odot}$ with dust obscuration factors $\gtrsim 100$. Galaxies in the U_nGR , BzK , and radio-detected SMG samples detected at $24 \mu\text{m}$ mostly follow the linear relation denoted by the solid line in Figure 11. For SMGs, $L_{\text{bol}} \approx L_{\text{IR}}$, so assuming the submillimeter estimates of L_{IR} (rather than the mid-IR estimates shown in Figure 11) will move the SMGs in a direction parallel to the $z \sim 2$ trend.

DRGs detected at $24 \mu\text{m}$ span a large range in L_{IR}/L_{1600} . About half the DRGs follow the linear trend established for optically selected galaxies at $z \sim 2$. The remaining half of DRGs have similar bolometric luminosities to those which follow the $z \sim 2$ trend, but the UV luminosities are a magnitude more attenuated than what we would have predicted from the Meurer et al. (1999) law. The SED analysis (§ 4) demonstrates that all of the DRGs which follow the $z \sim 2$ trend are all rela-

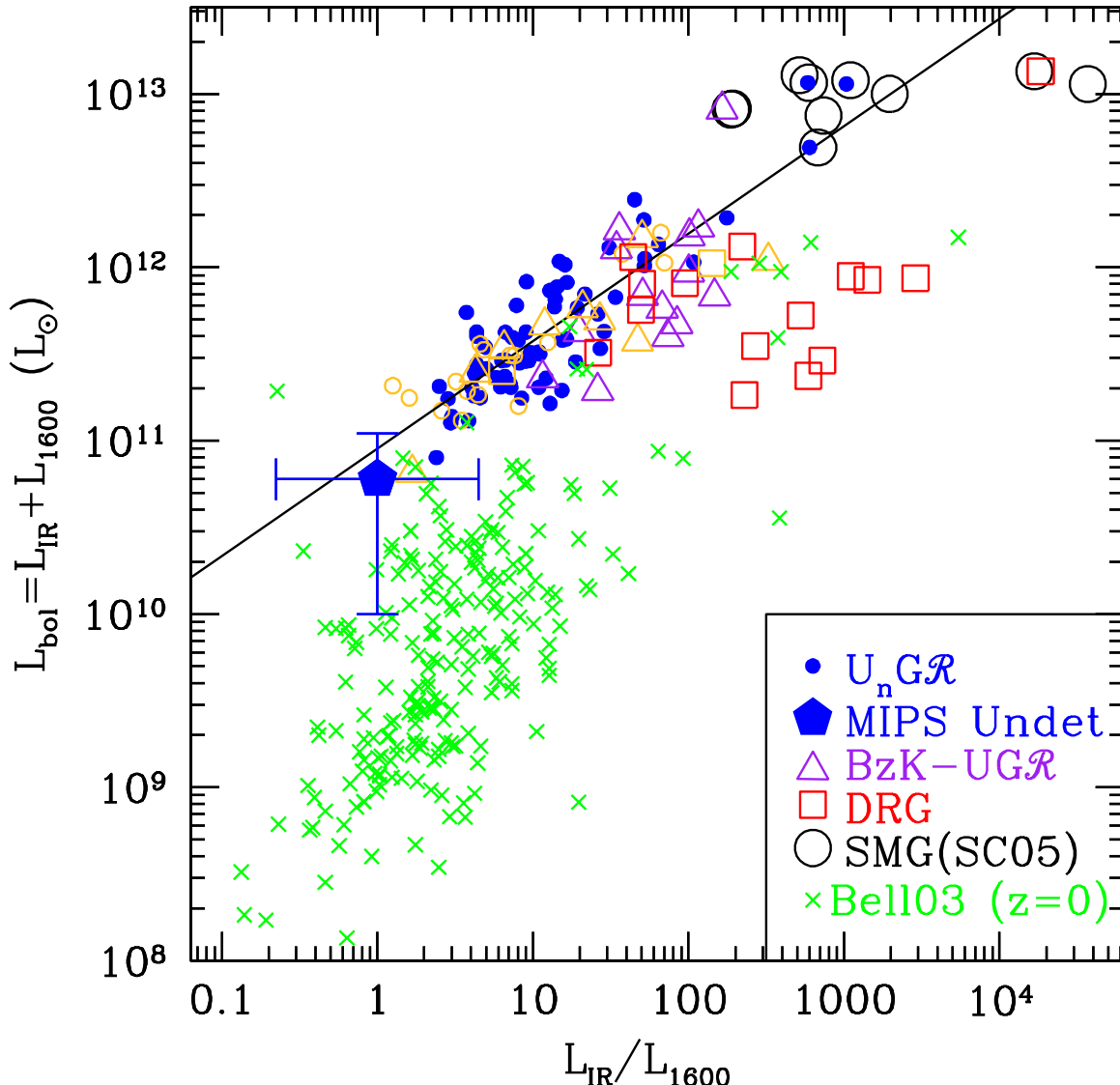


FIG. 11.— Bolometric luminosity, approximated as the sum of the IR and UV luminosities, versus dust obscuration. Shown are the distributions for $z \sim 2$ galaxies, and the solid line indicates the best-fit linear relation for spectroscopically confirmed U_nGR galaxies detected at $24 \mu\text{m}$. For comparison, the pentagon denotes the result for galaxies in the U_nGR sample undetected at $24 \mu\text{m}$, and the yellow symbols denote objects with inferred ages < 100 Myr. We also show local galaxies from the compilation of Bell (2003). Galaxies of a given bolometric luminosity are typically 8 – 10 times less dust obscured at high redshift than at the present epoch.

tively young galaxies (ages $\lesssim 2$ Gyr) and have lower stellar masses ($M^* \lesssim 10^{11} M_\odot$). In contrast, DRGs which are offset from the trend are all older (ages $\gtrsim 2$ Gyr) and all have masses $> 1.2 \times 10^{11} M_\odot$. The offset could be explained naturally if the dust masses of galaxies increase as they age, a natural consequence of star formation. Note that if the massive, metal-rich DRGs have stronger PAH flux for a given IR luminosity than the younger galaxies, then this would serve to only increase the offset between the massive DRGs and the $z \sim 2$ trend. In fact, stacking the X-ray data for the younger and older DRGs indicates they have very similar bolometric luminosities, confirming the results obtained by inferring L_{IR} from the PAH flux. The results of Figure 11 suggest that much of the dust in galaxies with the largest stellar masses was produced by star formation prior to the episode currently heating the dust. Therefore, such galaxies will have larger dust obscuration for a given bolometric luminosity. Assuming the two power-law conversion of

Elbaz et al. (2002) would result in a $z \sim 2$ trend with a slope 20% larger than given in Equation 5, but with approximately the same intercept within the uncertainties, so our conclusions would be unchanged.

As galaxies are enriched with dust as they age, then we expect to see an even greater difference in dust obscuration between $z \sim 2$ galaxies and those at the present epoch. To investigate this, we examined L_{bol} versus L_{IR}/L_{1600} for the sample of local galaxies compiled by Bell (2003), shown by crosses in Figure 11. The local sample includes the ULIRGs studied by Goldader et al. (2002). Unfortunately, the UV and IR data for local LIRG and ULIRGs are relatively sparse. However, of the small sample of local galaxies with $L_{bol} \gtrsim 10^{11} L_\odot$, almost all (10 of 11) lie to the right of the linear trend at $z \sim 2$ and at least half occupy the same region as the old, massive DRGs at $z \sim 2$. In fact, an interesting corollary to the above discussion is that massive, star-forming DRGs at $z \sim 2$ are more analogous to local ULIRGs than

bright SMGs at $z \sim 2$, both in terms of bolometric luminosity *and* dust-obscuration. Local ULIRGs undoubtedly carry a significant amount of dust into their current star formation episodes (e.g., Goldader et al. 2002), so it not surprising that they have similar dust-obscuration factors as massive, star-forming DRGs at $z \sim 2$. On the other hand, most galaxies lying on the $z \sim 2$ trend, including many bright SMGs, are likely undergoing their first major episode of star formation and have relatively low dust-to-gas ratios, unlike the more massive (offset) DRGs and local galaxies.

The offset between $z = 0$ and $z \sim 2$ galaxies can be seen at fainter bolometric luminosities where the local sample includes more galaxies ($10^{10} \lesssim L_{\text{bol}} \lesssim 10^{11}$). Restricting our analysis to galaxies in the Bell (2003) sample with L_{bol} comparable to those of $24 \mu\text{m}$ undetected $z \sim 2$ galaxies, we find that the local sample is on average ~ 10 times more dust obscured than $24 \mu\text{m}$ undetected galaxies at $z \sim 2$. Further, recent GALEX results indicate that local near-UV selected galaxies with $L_{\text{bol}} = 10^{11} L_{\odot}$ have a mean dust obscuration factor of ≈ 10 ; this is 8 times larger than the inferred dust obscuration of a $L_{\text{bol}} = 10^{11} L_{\odot}$ galaxy at $z = 2$ (Burgarella et al. 2005). To summarize, the important result from Figure 11 is that galaxies of a *given* bolometric luminosity are on average a factor of 8 – 10 less dust obscured at $z \sim 2$ than at the present epoch, confirming the trend first noted by Adelberger & Steidel (2000) between galaxies at $z = 0$, $z \sim 1$, and $z \sim 3$; this result is also suggested by the work of Calzetti & Heckman (1999). Again, this result could be anticipated if successive generations of star formation add to already existing dust within galaxies and/or if the dust distribution within galaxies becomes more compact with time (e.g., via the effects of mergers which tend to drive gas and dust to the central kpc of the system). The net result of dust enrichment and a more compact distribution of dust (e.g., after a merger event) is an increase in the dust column density towards star-forming regions. The relationship between dust obscuration and L_{bol} (i.e., Eq 5) indicates that for the mean L_{bol} of the $U_n\text{GR}$ selected sample of galaxies of $L_{\text{bol}} \sim 2.3 \times 10^{11} L_{\odot}$, the average dust obscuration is $\langle L_{\text{IR}}/L_{1600} \rangle \approx 4.6$. This factor is in excellent agreement with the mean attenuation of 4.5 – 5.0 inferred from stacked X-ray analyses (Reddy & Steidel 2004). One would observe a factor of 4 – 5 attenuation in a galaxy one order of magnitude less luminous at $z = 0$ than at $z \sim 2$. The implication is that, while it is true that a larger fraction of star formation at high redshifts occurs in dustier systems, the dust obscuration we observe for galaxies of a given L_{bol} has less of an impact on observations of high redshift galaxies than one would have surmised on the basis of present day galaxies.

8. PROPERTIES OF $24 \mu\text{m}$ FAINT GALAXIES

8.1. Ages and Masses of Faint $24 \mu\text{m}$ Galaxies

In addition to the information gleaned from the stacking analysis described above, we also have detailed information on the stellar populations of galaxies with faint mid-IR emission. Optical and near-IR selected galaxies undetected at $24 \mu\text{m}$ appear to have a distribution in ages which is similar to that of $24 \mu\text{m}$ detected galaxies (left panel of Figure 12), so young ages cannot explain why they are undetected at $24 \mu\text{m}$. Alternatively, although

we find a large range in inferred stellar mass of galaxies with $f_{24\mu\text{m}} < 8 \mu\text{Jy}$, the *mean* stellar mass of undetected objects is 0.4 dex lower in $\log M^*$ than $24 \mu\text{m}$ detected galaxies (right panel of Figure 12). Regardless of these small differences in the stellar populations of $24 \mu\text{m}$ detected and undetected sources, the X-ray data indicate that the primary reason why galaxies are undetected at $24 \mu\text{m}$ is because they have lower SFRs (Figure 4). We demonstrate in the next section how the rest-frame UV spectral properties of galaxies can be used to interpret their $24 \mu\text{m}$ emission.

8.2. Composite UV Spectra

A unique advantage of our optical $U_n\text{GR}$ selection is the efficiency with which we are able to obtain rest-frame UV spectra for these galaxies, and this spectroscopy allows for an independent probe of the physical conditions in the ISM. While the S/N of any individual spectrum is typically too low to accurately measure interstellar absorption line widths, we can take advantage of the large number of spectra by stacking them to create a higher S/N composite spectrum. To investigate differences in the ISM as a function of infrared luminosity, we constructed composite UV spectra for (a) the top quartile of $24 \mu\text{m}$ detected $U_n\text{GR}$ galaxies, and (b) all $U_n\text{GR}$ galaxies undetected at $24 \mu\text{m}$. In order to stack the spectra, we first de-redshifted them by the systemic redshift. The systemic redshift was inferred from a weighted combination of the measured absorption and/or emission line redshifts, following the procedure of Adelberger et al. (2003). We used the Rix et al. (2004) prescription to normalize the composite spectra to the underlying stellar continua. The detected and undetected composite spectra consist of 39 and 73 galaxies, respectively, and are shown in Figure 13. For comparison, the mean $24 \mu\text{m}$ flux of MIPS detected and undetected galaxies is $\langle f_{24 \mu\text{m}} \rangle \sim 100 \mu\text{Jy}$ and $\sim 3 \mu\text{Jy}$, respectively; both sub-samples have $\langle z \rangle \sim 2.1$. Table 3 lists the measured rest-frame equivalent widths of several interstellar absorption lines in the composite spectra. The primary difference between the rest-frame UV spectra of $24 \mu\text{m}$ detected and undetected galaxies is that the latter have interstellar absorption lines that are a factor of 2 weaker than the lines in the $24 \mu\text{m}$ detected galaxies. Because the line strengths are controlled by the combination of the velocity spread in outflowing interstellar material and the covering fraction of optically-thick material, this indicates that galaxies weak in mid-IR emission are likely to have more quiescent ISM than $24 \mu\text{m}$ -bright galaxies, a result expected if those galaxies undetected by MIPS have lower SFRs, and hence lower energy input into the ISM and a lower level of dust enrichment, than $24 \mu\text{m}$ detected galaxies.

Comparing the mid-IR detections with nondetections, we find the latter have significantly stronger Ly α emission than the former. The emergent Ly α profiles of galaxies will depend strongly on a number of physical parameters including the spectrum of UV radiation (i.e., the stellar IMF), presence of outflows, and dust covering fraction. Neglecting all of these effects, galaxies with larger SFRs will have stronger Ly α emission. However, given that the bolometric luminosity of star-forming galaxies scales with dust-obscuration (e.g., Figure 11), we might expect $24 \mu\text{m}$ detected galaxies to have larger dust col-

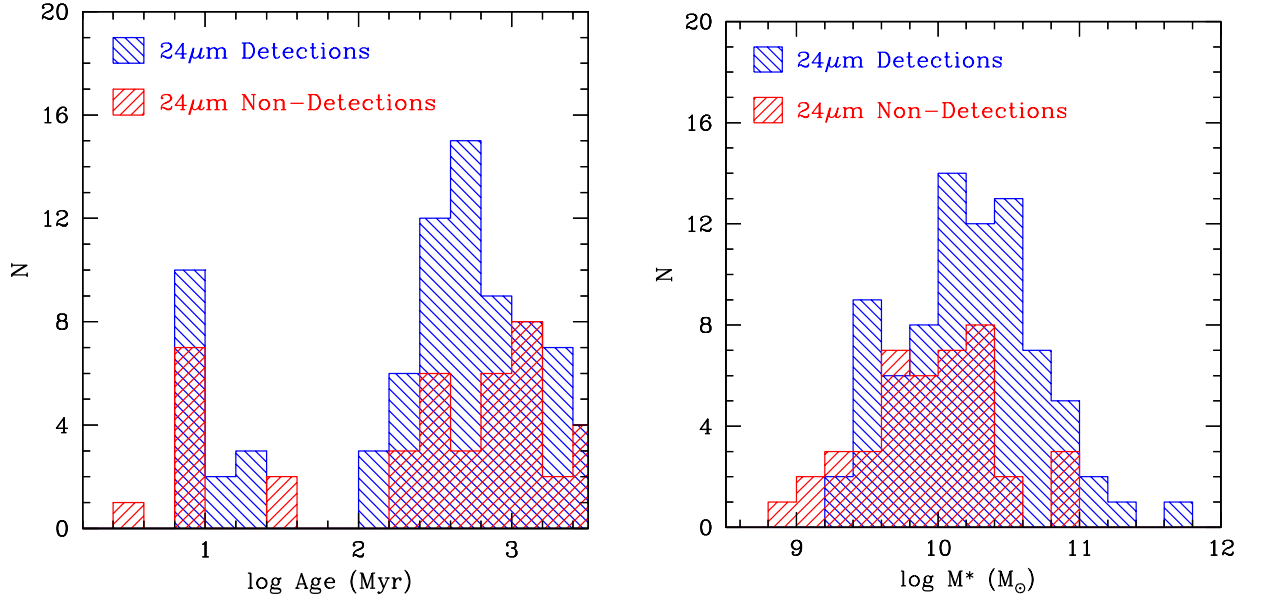


FIG. 12.— Histograms of the age (left panel) and mass (right panel) distributions for $24 \mu\text{m}$ detected and non-detected U_nGR galaxies with redshifts $1.5 < z < 2.6$. The age distributions of detected and non-detected U_nGR galaxies are similar. The mean of the mass distributions are offset such that undetected galaxies have $\langle \log M^* \rangle$ that is 0.4 dex lower than that of $24 \mu\text{m}$ detected galaxies.

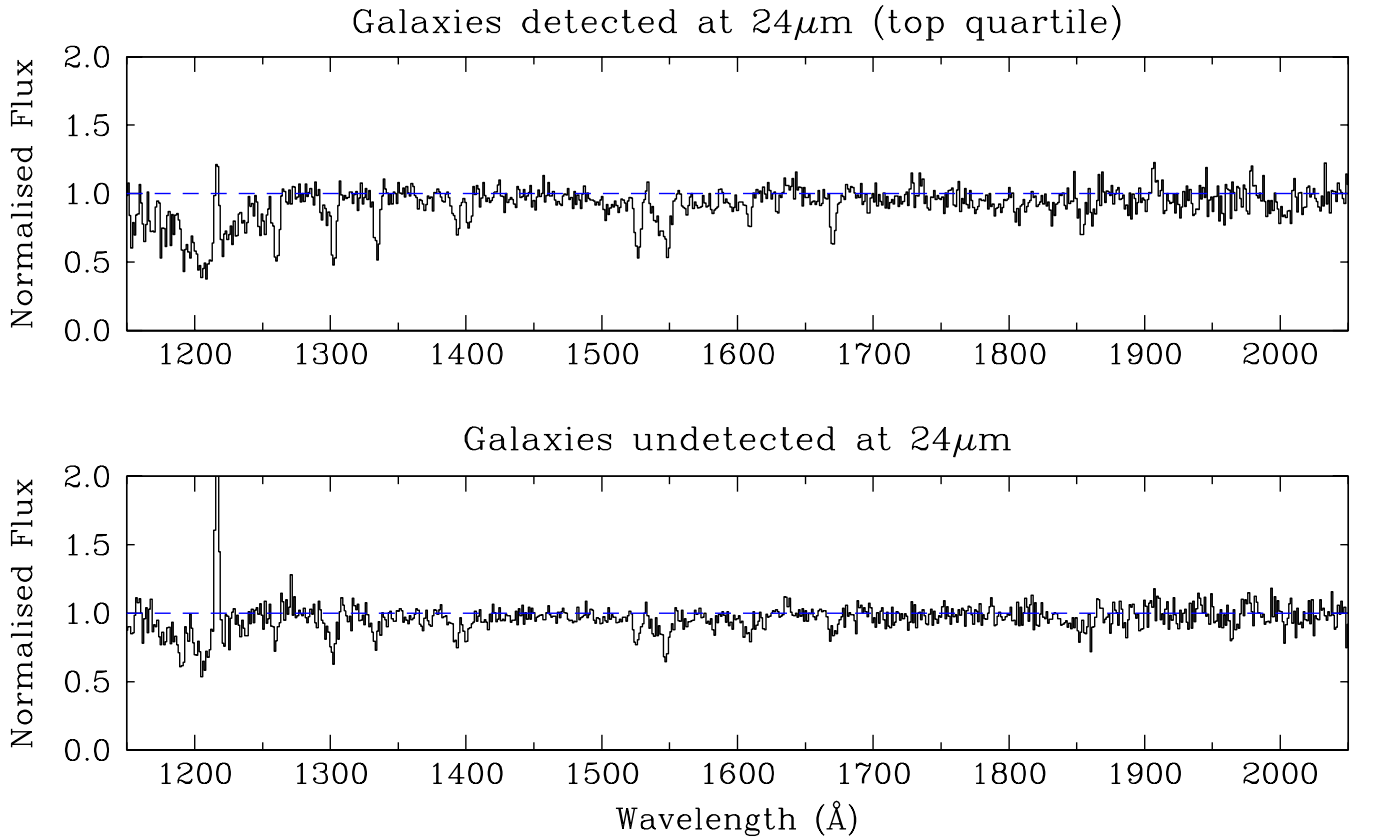


FIG. 13.— Normalized composite UV spectra for the 39 galaxies in the top quartile of $24 \mu\text{m}$ detected U_nGR galaxies (top) with $\langle f_{24\mu\text{m}} \rangle \sim 100 \mu\text{Jy}$ and 73 U_nGR galaxies undetected at $24 \mu\text{m}$ (bottom) with $\langle f_{24\mu\text{m}} \rangle \sim 3 \mu\text{Jy}$.

TABLE 3
INTERSTELLAR ABSORPTION LINE WAVELENGTHS AND
EQUIVALENT WIDTHS FOR 24 μm DETECTED AND
UNDETECTED U_nGR GALAXIES

Line	$\lambda_{\text{trans}}^{\text{a}}$	Detected W_λ^{b}	Undetected W_λ^{b}
Si II	1260.4	2.58	0.99
OI + Si II	1303.3	2.27	1.58
C II	1334.5	2.05	0.94
Si II	1526.7	2.36	1.32
Fe II	1608.5	0.87	1.15
Al II	1670.8	1.85	1.15
Al III	1854.7	1.66	0.55
Al III	1862.8	0.81	0.64

^aTransition wavelength in \AA .

^bMeasured rest-frame equivalent width in \AA .

umn densities than undetected galaxies; this may partly explain the absence of Ly α emission in 24 μm detected galaxies. In addition, the velocity spread of the ISM will also affect the emergent Ly α profile: the larger velocity spread in 24 μm detected galaxies, as indicated by their stronger interstellar absorption lines, implies most Ly α photons will have larger scattering path-lengths and are more likely to be attenuated by dust and/or scattered out of resonance (e.g., Hansen & Peng Oh 2005; Adelberger et al. 2003).

Finally, we note that the stacked X-ray analysis of 24 μm -undetected galaxies confirms they have lower SFRs than 24 μm -detected galaxies. Therefore, galaxies are undetected at rest-frame 5 – 8.5 μm primarily because they have lower SFRs and not because they are deficient in mid-IR PAH luminosity for a given L_{IR} . If such undetected galaxies had depressed MIR/IR flux ratios, we would not have expected to see as large a difference in the strengths of their interstellar absorption lines as compared with 24 μm detected galaxies.

9. MID-IR PROPERTIES OF MASSIVE GALAXIES AT $Z \sim 2$

The epoch between $z = 3$ and $z = 1$ appears to be the most active in terms of the buildup of stellar mass (e.g., Dickinson et al. (2003), see also § 1), but significant numbers of massive galaxies ($M^* \gtrsim 10^{11} L_\odot$) already appear to be in place by redshifts $z \sim 2$. The subsequent evolution of these massive galaxies and their relation to the local population of massive and passively evolving elliptical galaxies is an important question. It is useful to determine, therefore, what the mid-IR properties of massive galaxies tell us about their bolometric luminosities.

Figure 14 shows the bolometric luminosity of galaxies in the U_nGR , BzK , and DRG samples as a function of best-fit stellar mass. The mass modeling comes from the SED analysis where we have fit for the $R+JK_s+IRAC$ photometry assuming a constant star formation (CSF) model. As discussed elsewhere, the stellar mass is the most well determined parameter from the SED analysis and is relatively insensitive to the assumed star formation history (Shapley et al. 2005; Papovich et al. 2001). There are several interesting aspects worth considering in Figure 14. First, we note that galaxies with the youngest inferred ages ($\lesssim 100$ Myr) have low stellar masses ($M^* \lesssim 2 \times 10^{10} M_\odot$) and span a large range in

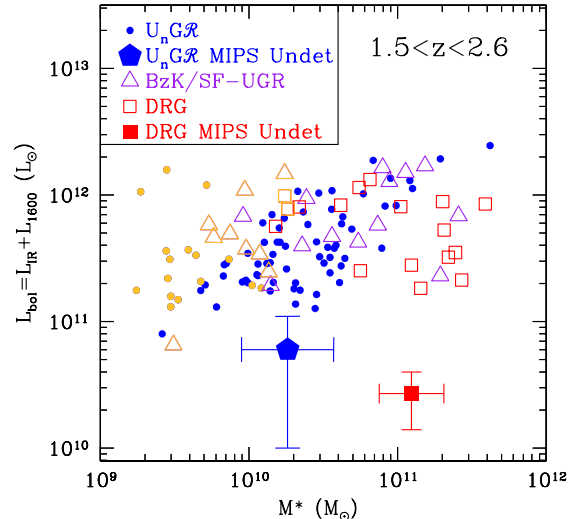


FIG. 14.— Inferred L_{bol} as a function of best-fit stellar mass assuming a CSF model for galaxies in the U_nGR , BzK , and DRG samples. We assumed a IR/MIR ratio of 17.2 to convert $L_{5-8.5\mu\text{m}}$ to L_{IR} . The large solid pentagon and square denote results for undetected U_nGR and the 7 undetected DRG galaxies, respectively. The light gray (yellow) symbols indicate 24 μm -detected galaxies with inferred ages ≤ 100 Myr.

bolometric luminosity from LIRG- to ULIRG-type galaxies. Among U_nGR galaxies with spectroscopic redshifts $1.5 < z < 2.6$, we note a trend of increasing L_{bol} with stellar mass; U_nGR galaxies with $M^* \gtrsim 10^{11} M_\odot$ have infrared luminosities typical of ULIRGs. The BzK/SF and DRG criteria cull $M^* \gtrsim 10^{11} M_\odot$ galaxies with a large range in bolometric luminosity, from $10^{11} L_\odot$ to $\gtrsim 10^{12} L_\odot$. Optically selected sources undetected at 24 μm have stellar masses similar to those of detected U_nGR galaxies, but with L_{bol} a factor of ~ 10 lower. As noted before, the 24 μm emission from these galaxies appears to be primarily dependent on their current star formation rate. Finally, we note that DRGs undetected at 24 μm have similar stellar masses as those which are detected ($M^* \gtrsim 10^{11} M_\odot$), but are on average 40 times less bolometrically luminous. As noted in § 5.2, these 24 μm -undetected DRGs have very red $(z-K)_{\text{AB}}$ colors. Their faint 24 μm emission corroborates the results of X-ray stacking analyses that indicate these galaxies have very little current star formation (Reddy et al. 2005).

The results of Figure 14 suggest that galaxies with large stellar masses at $z \sim 2$ span a large range in bolometric luminosity, from galaxies with little star formation to ULIRG-type systems. The range is likely larger than what one would infer from Figure 14 since we have excluded directly-detected X-ray sources that may be heavily star-forming galaxies and/or host AGN. Figure 14 suggests that $\gtrsim 70\%$ of massive galaxies ($M^* > 10^{11} M_\odot$) with redshifts $1.5 < z < 2.6$ in optical and near-IR surveys have $L_{\text{bol}} \gtrsim 3 \times 10^{11} L_\odot$ (or SFRs $\gtrsim 20 M_\odot \text{ yr}^{-1}$, assuming the SFR calibration of Kennicutt 1998a). Our results imply that most $1.5 < z < 2.6$ galaxies with large stellar masses ($M^* \gtrsim 10^{11} M_\odot$) have levels of star formation that exceed those of LIRGs.

10. DISCUSSION

10.1. Selection of LIRGs and ULIRGs at $z \sim 2$

In § 5.2 we showed that optical and near-IR selected samples to $\mathcal{R} = 25.5$, or $K_s = 22$, host galaxies with

a wide range in infrared luminosity, from a few times $10^{10} L_{\odot}$ up to the most luminous objects at these redshifts with $L_{\text{IR}} > 10^{12} L_{\odot}$. Typical galaxies in these samples have infrared luminosities in the range $10^{11} < L_{\text{IR}} < 10^{12} L_{\odot}$, similar in luminosity to, but with dust-obscuration a factor of ~ 10 lower than (see § 7), local LIRGs. One advantage of optical (i.e., rest-frame UV) selection of LIRGs and ULIRGs at high redshift is that it allows for the kind of efficient spectroscopic followup necessary to accurately interpret the nature of 24 μm emission from these galaxies. As shown in § 4, the K -correction depends sensitively on redshift such that even for “good” photometric redshift estimates with $\delta z/(1+z) \sim 0.1$, the corresponding uncertainty in the rest-frame 5–8.5 μm luminosity increases by a factor of 5. A particularly unique aspect of our study combining the optical sample with MIPS observations is that the spectroscopic database can be used to assess the physical conditions of the ISM in galaxies as function of L_{bol} , providing an additional method for probing the detailed nature of 24 μm galaxies at $z \sim 2$ (§ 8.2). Aside from the constraints on the mid-IR luminosities possible with spectroscopic redshifts, precise positions of sources from higher spatial resolution and shorter wavelength data enable the deblending of most $z \sim 2$ galaxies. The deblending procedure made possible by optical, near-IR, and *Spitzer* IRAC observations enable accurate identification and photometry of faint galaxies well below the MIPS 24 μm confusion limit and will provide a more complete “census” of the LIRG population at redshift $z \sim 2$ than possible using MIPS observations alone.

Further, selection by optical colors gives important information on the *unobscured* component of the star formation in galaxies and complements well the information on the obscured component probed by the 24 μm observations. Objects with lower star formation rates will have bolometric luminosities that are typically dominated by the observed UV emission and objects with larger star formation rates will have bolometric luminosities that are dominated by the observed IR emission. The transition between the UV and IR dominated regimes (i.e., where $L_{\text{IR}} = L_{1600}$) at $z \sim 2$ occurs for galaxies with $L_{\text{IR}} \approx 10^{11} L_{\odot}$, or about $0.3L^*$ (Figure 11). A comparison with the $z = 0$ sample of Bell (2003) shows that the bolometric luminosities begin to be dominated by IR emission (i.e., $L_{\text{IR}}/L_{1600} > 1$) for galaxies which are two orders of magnitude more luminous at $z \sim 2$ than at the present epoch. As discussed in § 7, this is plausibly explained as a result of higher dust-to-gas ratios in the local galaxies. More generally, galaxies of a given dust obscuration are anywhere from 2-100 times more luminous at $z \sim 2$ than locally (Figure 11), with the greatest difference for galaxies with relatively low $L_{\text{IR}}/L_{1600} \lesssim 20$. The implication of these observations is that while it is certainly true that a larger fraction of the star formation at high redshifts occurs in dustier galaxies, selection via rest-frame UV colors (and performing followup spectroscopy) is easier at high redshift than locally for galaxies at a given bolometric luminosity. Optical selection is therefore arguably the most promising and spectroscopically efficient method for selecting LIRGs (which undoubtedly account for a significant fraction of the star formation rate density and far-infrared background; e.g., Adelberger & Steidel 2000) at $z \sim 2$.

As demonstrated in § 5.2 and in Reddy et al. (2005), ULIRGs and SMGs at these redshifts also often appear in optical and near-IR selected samples; $\sim 50\%$ of the most luminous SMGs have enough unobscured star formation that they satisfy the $z \sim 2$ optical criteria (Chapman et al. 2005). Accounting for the obscured portion of star formation in these ultraluminous sources of course requires the longer wavelength data since rest-frame UV slopes underpredict their L_{IR} (§ 6). In some sense, 24 μm observations are a more powerful method of estimating L_{bol} of these ultra-luminous sources since their detection significance at 24 μm is typically 50–100 times larger and the beamsize is a factor of 9 smaller than at 850 μm . The ability to uniformly cover large areas of the sky with MIPS observations provides an additional advantage over current submillimeter surveys which suffer from areal and depth incompleteness, thus making it difficult to constrain the volumes probed. Using 24 μm observations to assess the global energetics of ultraluminous sources of course requires that we accurately calibrate the $L_{5-8.5\mu\text{m}}/L_{\text{IR}}$ ratios for these objects.

We have demonstrated that the typical galaxy in optical and near-IR samples of $z \sim 2$ galaxies has L_{IR} corresponding to that of LIRGs. A related issue is whether most LIRGs at $z \sim 2$ can be selected by their rest-frame UV or optical colors. A direct comparison of the number counts of MIPS sources to the number of 24 μm detected $U_n\text{GR}$ and BzK galaxies to 8 μJy (the GOODS-N MIPS 24 μm 3 σ sensitivity limit) is not possible since (a) we primarily relied on the K_s -band data to deblend sources in the 24 μm imaging and (b) the redshift distribution of MIPS sources to 8 μJy is not yet well established. Nonetheless, including both optical and near-IR selected LIRGs at $z \sim 2$ ensures that we must be reasonably “complete” for both optically-bright (and 24 μm -faint) LIRGs in the optical sample and optically-faint (and 24 μm -bright) LIRGs in the near-IR selected BzK and DRG samples. Galaxies with LIRG luminosities will predominantly have near-IR magnitudes bright enough to be considered in our analysis (i.e., $K_s \lesssim 21$ according to the left panel of Figure 8). Objects not selected by these various criteria will likely either fall at different redshifts, not have LIRG luminosities, and/or may be scattered out of the color selection windows due to photometric error (e.g., Reddy et al. 2005). As an example of one form of photometric scatter, in the course of the $z \sim 3$ Lyman Break Galaxy Survey, we relied on $U_n\text{GR}$ photometry based on images of the HDF-North field taken at the Palomar Hale 5 m Telescope (Steidel et al. 2003). We subsequently imaged a larger portion of the GOODS-North field using the Keck I Telescope (Steidel et al. 2004). Our photometric analysis indicates that of the BX/BM objects to $\mathcal{R} = 25.5$ identified in the Palomar imaging, about 76% were recovered as BX/BM objects in the Keck imaging. A small fraction of the remaining 24% were recovered using LBG selection. The level of scatter between different photometric realizations in other fields is also typically $\sim 25\%$ and is mostly due to the narrow photometric windows used to select BX/BM galaxies. Regardless of these photometric effects, it is highly unlikely that there exist large numbers of LIRGs at $z \sim 2$ with such different optical and near-IR properties that they would be completely absent from all the samples considered here. Finally, our knowledge of the

exact positions of optical and near-IR selected galaxies from the higher spatial resolution K_s -band and IRAC data allows us to mitigate the effects of confusion (see § 3), so we should be reasonably complete for galaxies which are detected at $24 \mu\text{m}$ to $8 \mu\text{Jy}$ but which might otherwise be confused with brighter sources. It is therefore reasonable to conclude that the LIRG population at $z \sim 2$ is essentially the same population of galaxies that are selected in optical and near-IR samples.

10.2. Mass Assembly at High Redshift

We demonstrated that LIRGs and ULIRGs are present over the full range of stellar mass, from $\sim 2 \times 10^9 M_\odot$ to $5 \times 10^{11} M_\odot$, for galaxies in the samples considered here (Figure 14). To assess the significance of the current star formation in the buildup of stellar mass, we have computed the specific star formation rate, ϕ , defined as the SFR per unit stellar mass. We show the observed ϕ for galaxies in our sample as function of stellar mass in Figure 15. The correlation between ϕ and M^* could have been predicted from Figure 14 since the range of L_{bol} is similar over the range of M^* considered here. We also note that the correlation is accentuated since (a) ϕ is not independent of M^* and (b) there are presumably galaxies with low ϕ and low M^* that would be missing from the optical and near-IR samples (irrespective of the MIPS detection limit). Furthermore, the upper envelope of points in Figure 15 is defined by our cut to exclude luminous AGN based on the *Chandra* X-ray data. Nonetheless, we find that star-forming galaxies with large stellar masses $M^* \gtrsim 10^{11} M_\odot$ without an AGN signature have specific SFRs that are 1 to 2 orders of magnitude lower than those of young galaxies (yellow symbols), implying that the current star formation contributes more significantly to the buildup of stellar mass in low mass galaxies than high mass galaxies at $z \sim 2$. This change in specific SFR as a function of mass has been observed at later epochs as well (e.g., Bell et al. 2005). The shifting of the relationship to lower specific SFRs at later epochs for galaxies with large stellar masses has been referred to as “downsizing” (Cowie et al. 1996).

The most massive, star-forming DRGs at these redshifts with large dust-to-gas ratios (see Figure 11) also have the lowest ϕ for MIPS-detected galaxies at $z \sim 2$. Papovich et al. (2005) demonstrate that the integrated specific SFR of these massive DRGs at $z \sim 2$ is ~ 2 magnitudes larger than for galaxies with similar masses ($M^* > 10^{11} M_\odot$) at lower redshifts $0.3 \leq z < 0.5$, based on a comparison with the COMBO-17 sample (Bell et al. 2005). This decrease in ϕ suggests that $M^* > 10^{11} M_\odot$ galaxies have built up most of their stellar mass by $z \sim 2$. In fact, the mass-doubling time becomes increasingly large for these massive galaxies if we assume the case of an exponentially declining star formation model. In this case, ϕ will evolve with time t as

$$\phi(t) = \frac{(1+f)\exp(-t/\tau)}{\tau[1-\exp(-t/\tau)]}, \quad (6)$$

where f is the ratio of the gas mass that is lost due to outflows to that formed in stars and τ is the star formation decay timescale as defined in § 4. Given some initial SFR, a CSF model (i.e., with $\tau = \infty$) will track straight through the points corresponding to galaxies

with $M^* \gtrsim 10^{11} M_\odot$, but such a model would predict a ϕ at $z \sim 0.4$ that is ~ 5 times larger than observed at $z \sim 0.4$ in the COMBO-17 survey (Bell et al. 2005). Therefore, a declining star-formation history may be more appropriate for describing the future evolution of galaxies with large stellar masses at $z \sim 2$. In particular, Erb et al. (2006a) find that a model that assumes a super-solar yield of metals (i.e., ratio of mass of metals ejected into the ISM to mass of metals locked in long-lived stars) of $y = 1.5 Z_\odot$ and an outflow rate of $4 \times \text{SFR}$ ($f = 4$) appears to best-fit the observed metallicities of U_nGR galaxies at $z \sim 2$ as a function of gas fraction. If all star-forming galaxies at $z \sim 2$ follow a similar evolutionary track as the $M^* > 10^{11} M_\odot$ galaxies (i.e., follow an exponentially declining star formation history with large outflow rate), then the scatter of galaxies with a given specific SFR simply reflects the range in the final stellar masses and dark matter halo masses (see also discussion in Erb et al. 2006a).

We can directly relate the specific SFR ϕ with the cold gas fraction, $\mu \equiv M_{\text{gas}}/(M_{\text{gas}} + M^*)$. If we assume that the SFR is proportional to the cold gas mass, M_{gas} , to the 1.4 power according to the Schmidt law (Kennicutt 1998b), then

$$\phi \propto \frac{M_{\text{gas}}^{1.4}}{M^*}. \quad (7)$$

It then follows that

$$\phi = C \frac{\mu^{1.4}}{1-\mu}, \quad (8)$$

where C is a constant that depends on the constant of proportionality between the SFR and gas mass surface densities in the Schmidt law and the total gas mass at virialization (i.e., when star formation commences). There is a one-to-one correspondence between the specific SFR, ϕ , and gas fraction, μ , such that galaxies with large specific SFRs will have a larger fraction of cold gas than galaxies with small specific SFRs. Erb et al. (2006b) demonstrate that μ decreases as a function of stellar mass for a large sample of U_nGR galaxies with $\text{H}\alpha$ spectroscopy, with a mean μ across the sample of $\langle \mu \rangle \sim 0.5$. The mean specific SFR for these galaxies is $\langle \phi \rangle \sim 3 \text{ Gyr}^{-1}$. Using these mean values to estimate C , we show the range of μ on the right-hand axis of Figure 15. Young galaxies with ages less than 100 Myr in our sample also have the largest gas fractions ($\mu \sim 0.6 - 0.9$) and largest specific SFRs (Figure 15) compared with older galaxies at $z \sim 2$. These results strongly suggest that the young galaxies have large reservoirs of cold gas and have just begun forming stars. Similarly, galaxies with the largest stellar masses have lower specific SFRs and therefore lower cold gas fractions ($\mu \sim 0.1 - 0.3$) and are likely to cease star-formation in a relatively short time. The correlation between ϕ and M^* revealed by Figure 15 is actually expected from the trend between μ and M^* inferred from the $\text{H}\alpha$ spectroscopic analysis of Erb et al. (2006b). Furthermore, Erb et al. (2006a) find a tight trend between metallicity and gas fraction such that galaxies with lower μ are more metal-rich. These galaxies will therefore be more dust-obscured since metallicity is directly proportional to dust-to-gas ratio. Our analysis confirms our expectation that the most dust-obscured objects at $z \sim 2$ (i.e.,

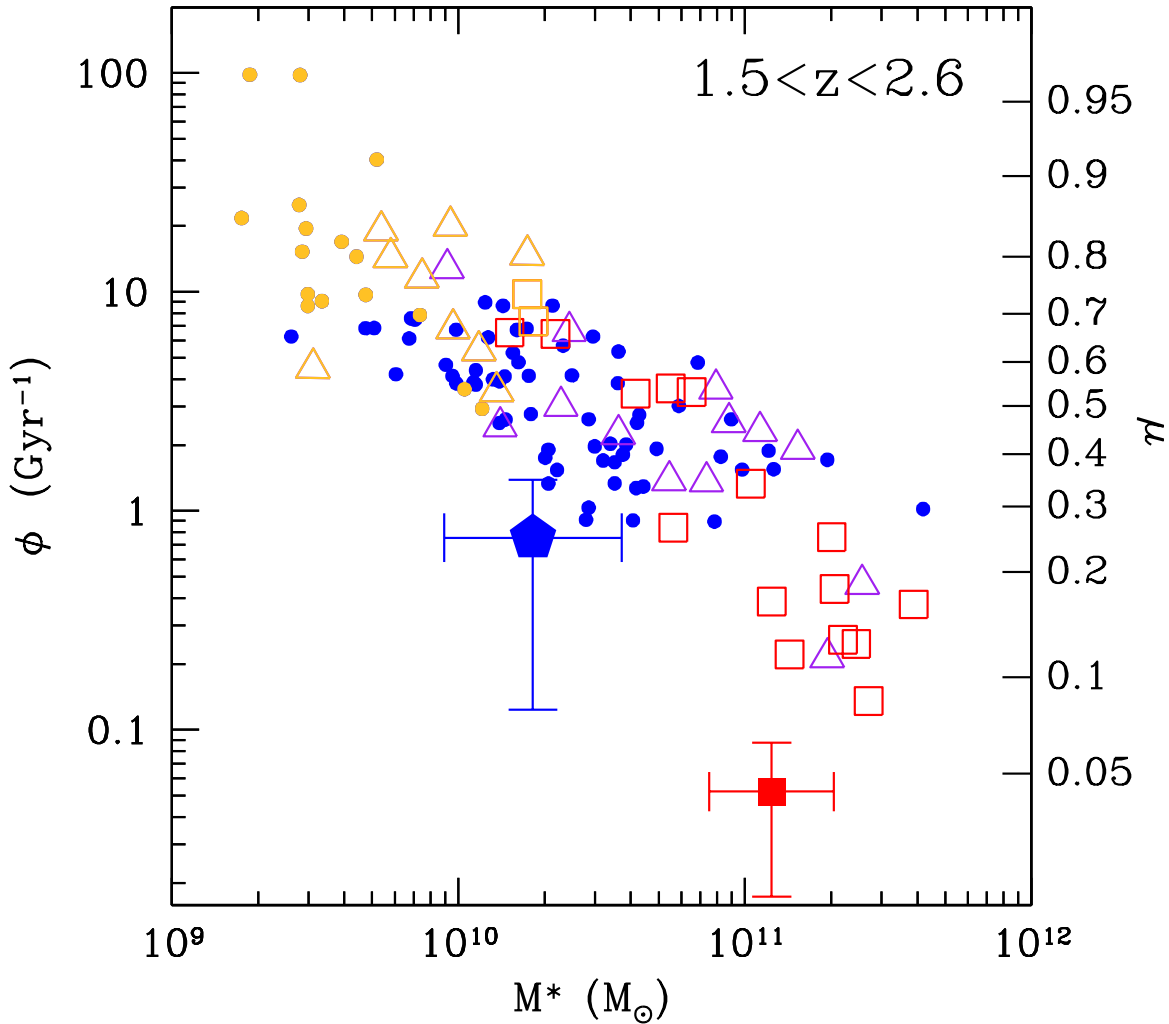


FIG. 15.— Specific SFR, ϕ , as a function of stellar mass for galaxies in the samples considered here. Symbols are the same as in Figure 14 (yellow symbols indicate galaxies with inferred ages $\lesssim 100$ Myr). The right-hand axis indicates the gas fraction μ associated with galaxies of a given ϕ .

the DRGs with the largest dust-to-gas ratios, Figure 11) also have low gas fractions as demonstrated in Figure 15. Figure 15 indicates that the trend in gas fraction versus stellar mass (or, metallicity versus gas fraction) found for U_nGR -selected galaxies with $H\alpha$ spectroscopy (Erb et al. 2006a) also applies to galaxies selected by their near-IR colors.

Combining the optical and near-IR samples, we find a wide range in the evolutionary state of galaxies at $z \sim 2$, from those which are just starting to form stars to those which have already accumulated most of their stellar mass and are about to become passive or already are. Almost all DRGs with the reddest $(z - K)_{AB}$ color ($(z - K)_{AB} > 3$) are undetected at $24 \mu\text{m}$ and in the deep *Chandra* X-ray data (e.g., see right panel of Figure 8 and Figure 16 in Reddy et al. 2005). The specific SFRs of these red DRGs are the lowest observed for the $z \sim 2$ galaxies considered here; they have cold gas fractions of less than 5%, confirming that they have essentially shut-off star formation by $z \sim 2$. The star-forming DRGs with $M^* > 10^{11} M_\odot$ (which are dusty and metal-rich as inferred from their large dust-to-gas ratios; cf., Figure 11) are likely to reach this passively-evolving state by redshifts $z \lesssim 1.5$. A simple model which assumes a

high outflow rate proportional to the SFR and exponentially declining star formation history (i.e., the model which appears to best-fit the observed metallicities of galaxies as function of gas fraction; Erb et al. 2006a) is sufficient to explain the presence of galaxies with large stellar masses and little star formation by $z \sim 2$ without invoking AGN feedback, despite the fact that a large AGN fraction of $\sim 25\%$ is observed among galaxies with large stellar masses (Reddy et al. 2005).

11. CONCLUSIONS

We use *Spitzer* MIPS data to examine the bolometric luminosities and extinction properties of optical and near-IR selected galaxies at redshifts $1.5 \lesssim z \lesssim 2.6$ in the GOODS-North field. At these redshifts, the mid-IR ($5 - 8.5 \mu\text{m}$) features associated with polycyclic aromatic hydrocarbon (PAH) emission, which are ubiquitous in local and $z \sim 1$ star-forming galaxies, are shifted into the MIPS $24 \mu\text{m}$ filter. Extensive multi-wavelength data in the GOODS-North field, including very deep *Chandra* X-ray data, allow us to test the validity of inferring the bolometric luminosities of high redshift galaxies from their rest-frame $5 - 8.5 \mu\text{m}$ emission. Galaxies at $z \sim 2$ are selected by their optical (U_nGR) and near-IR (BzK and $J - K_s$) colors, and for comparison we also consider radio-

detected submillimeter galaxies (SMGs; Chapman et al. 2005). The optically-selected sample is advantageous because we have knowledge of the precise redshifts of $\gtrsim 300$ galaxies from spectroscopy, allowing for the most accurate estimates of the rest-frame mid-IR luminosities of $z \sim 2$ galaxies. In addition to our spectroscopic sample, we use deep optical, near-IR, and *Spitzer* IRAC data to derive photometric redshifts for *BzK* galaxies and those with red $J - K_s > 2.3$ colors (Distant Red Galaxies; DRGs). The principle conclusions of this study are as follows:

1. Using local templates to K -correct the observed $24 \mu\text{m}$ fluxes, we find that the rest-frame $5 - 8.5 \mu\text{m}$ luminosity ($L_{5-8.5\mu\text{m}}$) of $z \sim 2$ galaxies correlates well with their stacked X-ray emission. A subset of galaxies with $\text{H}\alpha$ measurements have $\text{H}\alpha$ -inferred bolometric luminosities that correlate very well with their $L_{5-8.5\mu\text{m}}$ -inferred bolometric luminosities (with a scatter of 0.2 dex). These observations suggest that $L_{5-8.5\mu\text{m}}$ provides a reliable estimate of L_{IR} for most star forming galaxies at $z \sim 2$.

2. We find that the optical and near-IR selected $z \sim 2$ galaxies span a very wide range in infrared luminosity from LIRG to ULIRG objects. We find a mean infrared luminosity of $\langle L_{\text{IR}} \rangle \sim 2 \times 10^{11} L_{\odot}$ for galaxies in the optical and near-IR samples, in excellent agreement with the value obtained from a stacked X-ray analysis. The optical and near-IR selected star-forming galaxies likely account for a significant fraction of the LIRG population at $z \sim 2$. Galaxies with $K_s < 20$ have L_{IR} greater than 2 times that of galaxies with $K_s > 20.5$. Non-AGN galaxies with the reddest near-IR colors ($(z - K)_{\text{AB}} > 3$) are mostly undetected at $24 \mu\text{m}$ suggesting they have low SFRs, a conclusion supported by stacked X-ray analyses.

3. We demonstrate using $24 \mu\text{m}$ and X-ray stacking analyses that galaxies undetected to $f_{24\mu\text{m}} \sim 8 \mu\text{Jy}$ are faint because they have lower SFRs and/or lower obscuration than $24 \mu\text{m}$ detected galaxies, and not because they are deficient in PAH emission at a given L_{IR} . We infer that typically half of the bolometric luminosity of these $24 \mu\text{m}$ -undetected galaxies is emitted in the UV. Comparing the rest-frame UV composite spectra of $24 \mu\text{m}$ -undetected galaxies with those in the top quartile of detected objects shows that the latter have low-ionization interstellar absorption lines that are ~ 2 times stronger than the former, indicating some combination of more turbulent interstellar media and a larger neutral gas covering fraction. This is consistent with our conclusion that galaxies undetected at $24 \mu\text{m}$ have lower SFRs than $24 \mu\text{m}$ -detected galaxies, and therefore a lower input of kinetic energy and dust into their ISM.

4. The $24 \mu\text{m}$ (and deep X-ray) data indicate that galaxies whose current star-formation episodes are older than 100 Myr and have infrared luminosities $10^{10} \lesssim L_{\text{IR}} \lesssim 10^{12} L_{\odot}$ appear to follow the local relation between rest-frame UV slope and dust obscuration, implying that such galaxies at $z \sim 2$ have moderate amounts of dust extinction and that their UV slopes can be used to infer their extinction. Galaxies younger than 100 Myr have rest-frame UV colors that are redder than expected given their inferred L_{IR} , indicating they may obey a steeper extinction law. These young galaxies have the lowest stellar masses, but span the same range in bolometric luminosity as galaxies with larger stellar masses.

5. Galaxies with $L_{\text{bol}} \gtrsim 10^{12} L_{\odot}$, including radio-

detected SMGs, are typically $\sim 10 - 100$ times more dust obscured than their UV spectral slopes would indicate, assuming their $850 \mu\text{m}$ -inferred infrared luminosities. The $24 \mu\text{m}$ -inferred infrared luminosities of radio-detected SMGs are systematically a factor of 2–10 times lower than those predicted by their $850 \mu\text{m}$ fluxes; adopting the $24 \mu\text{m}$ estimates implies dust attenuation factors that are $\sim 5 - 50$ times larger than their UV spectral slopes would indicate. Regardless, such galaxies will often be blue enough to satisfy the $U_n\mathcal{GR}$ criteria, so finding these dust obscured galaxies in optical surveys is not uncommon.

6. A comparison between the dust obscuration in $z \sim 2$ and $z = 0$ galaxies suggests that galaxies of a *given* bolometric luminosity are much less dust obscured (by a factor of $\sim 8 - 10$) at high redshift than at the present epoch. This result is expected (a) as galaxies age and go through successive generations of star formation and dust production and (b) if the distribution of dust and star formation in galaxies becomes more compact over time (e.g., through mergers or interactions) resulting in greater dust column densities towards star-forming regions. We find that star-forming Distant Red Galaxies (DRGs) with stellar masses $M^* \gtrsim 10^{11} M_{\odot}$ and ages $\gtrsim 2$ Gyr have bolometric luminosities and dust-obscuration factors similar to those of local ULIRGs, suggesting that such DRGs, like local ULIRGs, carry relatively large amounts of dust into their current episodes of star formation.

7. Galaxies with the largest stellar masses at $z \sim 2$ ($M^* \gtrsim 10^{11} M_{\odot}$) also span a large range in bolometric luminosity, from those which have red near-IR colors ($(z - K)_{\text{AB}} > 3$) with little current star formation to those ULIRG objects found among optical and near-IR selected massive galaxies. Our results suggest $\gtrsim 70\%$ of massive galaxies ($M^* \gtrsim 10^{11} M_{\odot}$) in optical and near-IR surveys with redshifts $1.5 < z < 2.6$ have $L_{\text{bol}} \gtrsim 3 \times 10^{11} L_{\odot}$ (SFRs $\gtrsim 20 M_{\odot} \text{ yr}^{-1}$), comparable to and exceeding the luminosity of LIRGs.

8. Similar to lower redshift studies, we find a trend between specific SFR (SFR per unit stellar mass) and stellar mass at $z \sim 2$ which indicates that the observed star formation contributes more to the buildup of stellar mass in galaxies with low stellar masses than in those with larger stellar masses at $z \sim 2$. This trend between specific SFR and stellar mass indicates a strong decrease in cold gas fraction as function of stellar mass, consistent with results from near-IR spectroscopic observations, and suggests that galaxies with large stellar masses ($M^* > 10^{11} M_{\odot}$) at $z \sim 2$ will quickly cease star formation. Combining optical and near-IR selected samples, we find a large range in the evolutionary state of galaxies at $z \sim 2$, from those which have just begun to form stars and which have large gas fractions to those which are old, massive, and have little remaining cold gas.

We thank Natascha Förster Schreiber and Helene Roussel for providing their ISO spectra of local galaxies, and David Elbaz for providing an electronic catalog of the mid-IR and IR luminosities of local star-forming galaxies. We also thank the referee, Emeric Le Floch, for useful comments. The work presented here has been

supported by grant AST 03-07263 from the National Science Foundation and by the David and Lucile Packard Foundation. We made use of the NASA/IPAC Extra-

galactic Database (NED), which is operated by the Jet Propulsion Laboratory, California Institute of Technology, under contract with NASA.

REFERENCES

- Adelberger, K. L. & Steidel, C. C. 2000, *ApJ*, 544, 218
 Adelberger, K. L., Steidel, C. C., Shapley, A. E., Hunt, M. P., Erb, D. K., Reddy, N. A., & Pettini, M. 2004, *ApJ*, 607, 226
 Adelberger, K. L., Steidel, C. C., Shapley, A. E., & Pettini, M. 2003, *ApJ*, 584, 45
 Alexander, D. M., Bauer, F. E., Chapman, S. C., Smail, I., Blain, A. W., Brandt, W. N., & Ivison, R. J. 2005, submitted to *ApJ*
 Alexander, D. M., et al. 2003, *AJ*, 126, 539
 Almaini, O., Lawrence, A., & Boyle, B. J. 1999, *MNRAS*, 305, L59
 Alonso-Herrero, A., Takagi, T., Baker, A. J., Rieke, G. H., Rieke, M. J., Imanishi, M., & Scoville, N. Z. 2004, *ApJ*, 612, 222
 Armus, L., et al. 2004, *ApJS*, 154, 178
 Baker, A. J., Lutz, D., Genzel, R., Tacconi, L. J., & Lehnert, M. D. 2001, *A&A*, 372, L37
 Barger, A. J., Cowie, L. L., Sanders, D. B., Fulton, E., Taniguchi, Y., Sato, Y., Kawara, K., & Okuda, H. 1998, *Nature*, 394, 248
 Bell, E. F. 2002, *ApJ*, 577, 150
 —. 2003, *ApJ*, 586, 794
 Bell, E. F., et al. 2005, *ApJ*, 625, 23
 Benítez, N. 2000, *ApJ*, 536, 571
 Bolzonella, M., Miralles, J.-M., & Pelló, R. 2000, *A&A*, 363, 476
 Boselli, A., et al. 1998, *A&A*, 335, 53
 Brandt, W. N., Hornschemeier, A. E., Schneider, D. P., Alexander, D. M., Bauer, F. E., Garmire, G. P., & Vignali, C. 2001, *ApJ*, 558, L5
 Bruzual, G. & Charlot, S. 2003, *MNRAS*, 344, 1000
 Burgarella, D., Perez-Gonzalez, P., Buat, V., Takeuchi, T. T., Lauger, S., Rieke, G., & Ilbert, O. 2005, *ArXiv Astrophysics e-prints*
 Calzetti, D., Armus, L., Bohlin, R. C., Kinney, A. L., Koornneef, J., & Storchi-Bergmann, T. 2000, *ApJ*, 533, 682
 Calzetti, D. & Heckman, T. M. 1999, *ApJ*, 519, 27
 Chapman, S. C., Blain, A. W., Smail, I., & Ivison, R. J. 2005, *ApJ*, 622, 772
 Charmandaris, V., Mirabel, I. F., Tran, D., Laurent, O., Cesarsky, C. J., Gallais, P., Sauvage, M., & Vigroux, L. 1997, in *Extragalactic Astronomy in the Infrared*, 283–+
 Cimatti, A., et al. 2002a, *A&A*, 392, 395
 Cimatti, A., et al. 2002b, *A&A*, 391, L1
 Condon, J. J., Anderson, M. L., & Helou, G. 1991, *ApJ*, 376, 95
 Cowie, L. L., Songaila, A., Hu, E. M., & Cohen, J. G. 1996, *AJ*, 112, 839
 Daddi, E., Cimatti, A., Renzini, A., Fontana, A., Mignoli, M., Pozzetti, L., Tozzi, P., & Zamorani, G. 2004, *ApJ*, 617, 746
 Daddi, E., et al. 2005, *astro-ph/0507504*
 Dale, D. A., Helou, G., Contursi, A., Silbermann, N. A., & Kolhatkar, S. 2001, *ApJ*, 549, 215
 Dale, D. A., et al. 2000, *AJ*, 120, 583
 Desert, F.-X., Boulanger, F., & Puget, J. L. 1990, *A&A*, 237, 215
 Di Matteo, T., Croft, R. A. C., Springel, V., & Hernquist, L. 2003, *ApJ*, 593, 56
 Dickinson, M., Papovich, C., Ferguson, H. C., & Budavári, T. 2003, *ApJ*, 587, 25
 Elbaz, D., Cesarsky, C. J., Chantal, P., Aussel, H., Franceschini, A., Fadda, D., & Chary, R. R. 2002, *A&A*, 384, 848
 Engelbracht, C. W., Gordon, K. D., Rieke, G. H., Werner, M. W., Dale, D. A., & Latter, W. B. 2005, *ApJ*, 628, L29
 Erb, D. K., Shapley, A. E., Pettini, M., Steidel, C. C., Reddy, N. A., & Adelberger, K. L. 2006a, *astro-ph/0602473*
 —. 2006b, submitted to *ApJ*
 —. 2006c, submitted to *ApJ*
 Förster Schreiber, N. M., Roussel, H., Sauvage, M., & Charmandaris, V. 2004a, *A&A*, 419, 501
 Förster Schreiber, N. M., Sauvage, M., Charmandaris, V., Laurent, O., Gallais, P., Mirabel, I. F., & Vigroux, L. 2003, *A&A*, 399, 833
 Förster Schreiber, et al. 2004b, *ApJ*, 616, 40
 Fabian, A. C. & Iwasawa, K. 1999, *MNRAS*, 303, L34
 Fadda, D., Flores, H., Hasinger, G., Franceschini, A., Altieri, B., Cesarsky, C. J., Elbaz, D., & Ferrando, P. 2002, *A&A*, 383, 838
 Fadda, D., et al. 2006, submitted to *AJ*
 Fan, X., et al. 2001, *AJ*, 121, 54
 Flores, H., et al. 1999, *ApJ*, 517, 148
 Franx, M., et al. 2003, *ApJ*, 587, L79
 Genzel, R. & Cesarsky, C. J. 2000, *ARA&A*, 38, 761
 Giavalisco, M., et al. 2004, *ApJ*, 600, L93
 Giavalisco, M., Koratkar, A., & Calzetti, D. 1996, *ApJ*, 466, 831
 Goldader, J. D., Meurer, G., Heckman, T. M., Seibert, M., Sanders, D. B., Calzetti, D., & Steidel, C. C. 2002, *ApJ*, 568, 651
 Haas, M., Klaas, U., Müller, S. A. H., Chini, R., & Coulson, I. 2001, *A&A*, 367, L9
 Hansen, M. & Peng Oh, S. 2005, *astro-ph/0507586*
 Helou, G., Khan, I. R., Malek, L., & Boehmer, L. 1988, *ApJS*, 68, 151
 Helou, G., Lu, N. Y., Werner, M. W., Malhotra, S., & Silbermann, N. 2000, *ApJ*, 532, L21
 Helou, G., Malhotra, S., Hollenbach, D. J., Dale, D. A., & Contursi, A. 2001, *ApJ*, 548, L73
 Hogg, D. W., Tremonti, C. A., Blanton, M. R., Finkbeiner, D. P., Padmanabhan, N., Quintero, A. D., Schlegel, D. J., & Wherry, N. 2005, *ApJ*, 624, 162
 Houck, J. R., et al. 2005, *ApJ*, 622, L105
 Hughes, D. H., et al. 1998, *Nature*, 394, 241
 Kennicutt, R. C. 1998a, *ARA&A*, 36, 189
 —. 1998b, *ApJ*, 498, 541
 Kong, X., Charlot, S., Brinchmann, J., & Fall, S. M. 2004, *MNRAS*, 349, 769
 Laird, E., Nandra, K., Adelberger, K. L., Steidel, C. C., & Reddy, N. A. 2005, *astro-ph/0501411*
 Lehmer, B. D., et al. 2005, *AJ*, 129, 1
 Lilly, S. J., Le Fevre, O., Hammer, F., & Crampton, D. 1996, *ApJ*, 460, L1+
 Madau, P., Ferguson, H. C., Dickinson, M. E., Giavalisco, M., Steidel, C. C., & Fruchter, A. 1996, *MNRAS*, 283, 1388
 Makovoz, D. & Marleau, F. R. 2005, *astro-ph/0507007*
 Meurer, G. R., Heckman, T. M., & Calzetti, D. 1999, *ApJ*, 521, 64
 Nandra, K., Mushotzky, R. F., Arnaud, K., Steidel, C. C., Adelberger, K. L., Gardner, J. P., Teplitz, H. I., & Windhorst, R. A. 2002, *ApJ*, 576, 625
 Normand, P., Rouan, D., Lacombe, F., & Tiphene, D. 1995, *A&A*, 297, 311
 Papovich, C., Dickinson, M., & Ferguson, H. C. 2001, *ApJ*, 559, 620
 Papovich, C., et al. 2005, *astro-ph/0511289*
 Persic, M., Rephaeli, Y., Braitto, V., Cappi, M., Della Ceca, R., Franceschini, A., & Gruber, D. E. 2004, *A&A*, 419, 849
 Pozzi, F., et al. 2004, *ApJ*, 609, 122
 Puget, J. L. & Leger, A. 1989, *ARA&A*, 27, 161
 Ranalli, P., Comastri, A., & Setti, G. 2003, *A&A*, 399, 39
 Reddy, N. A., Adelberger, K. L., Steidel, C. C., Shapley, A., Pettini, M., & Erb, D. K. 2006, in preparation
 Reddy, N. A., Erb, D. K., Steidel, C. C., Shapley, A., Adelberger, K. L., & Pettini, M. 2005, *ApJ*, 633, 748
 Reddy, N. A. & Steidel, C. C. 2004, *ApJ*, 603, L13
 Rix, S. A., Pettini, M., Leitherer, C., Bresolin, F., Kudritzki, R.-P., & Steidel, C. C. 2004, *ApJ*, 615, 98
 Roussel, H., Sauvage, M., Vigroux, L., & Bosma, A. 2001, *A&A*, 372, 427
 Rowan-Robinson, M., et al. 2004, *MNRAS*, 351, 1290
 Rudnick, G., et al. 2003, *ApJ*, 599, 847
 Sanders, D. B. & Mirabel, I. F. 1996, *ARA&A*, 34, 749
 Shapley, A. E., Steidel, C. C., Erb, D. K., Reddy, N. A., Adelberger, K. L., Pettini, M., Barmby, P., & Huang, J. 2005, *ApJ*, 626, 698
 Shaver, P. A., Wall, J. V., Kellermann, K. I., Jackson, C. A., & Hawkins, M. R. S. 1996, *Nature*, 384, 439
 Smail, I., Ivison, R. J., & Blain, A. W. 1997, *ApJ*, 490, L5+
 Smail, I., Ivison, R. J., Blain, A. W., & Kneib, J.-P. 2002, *MNRAS*, 331, 495
 Soifer, B. T., Sanders, D. B., Madore, B. F., Neugebauer, G., Danielson, G. E., Elias, J. H., Lonsdale, C. J., & Rice, W. L. 1987, *ApJ*, 320, 238
 Steidel, C. C., Adelberger, K. L., Giavalisco, M., Dickinson, M., & Pettini, M. 1999, *ApJ*, 519, 1

- Steidel, C. C., Adelberger, K. L., Shapley, A. E., Pettini, M., Dickinson, M., & Giavalisco, M. 2003, *ApJ*, 592, 728
- Steidel, C. C., Shapley, A. E., Pettini, M., Adelberger, K. L., Erb, D. K., Reddy, N. A., & Hunt, M. P. 2004, *ApJ*, 604, 534
- Sturm, E., Lutz, D., Tran, D., Feuchtgruber, H., Genzel, R., Kunze, D., Moorwood, A. F. M., & Thornley, M. D. 2000, *A&A*, 358, 481
- Tielens, A. G. G. M., Hony, S., van Kerckhoven, C., & Peeters, E. 1999, in *ESA SP-427: The Universe as Seen by ISO*, 579—+ van Dokkum, P. G., et al. 2004, *ApJ*, 611, 703
- Yan, L., et al. 2005, *ApJ*, 628, 604
- Yun, M. S., Reddy, N. A., & Condon, J. J. 2001, *ApJ*, 554, 803